

Eco-Evolutionary Theory and Insect Outbreaks

David J. Páez,^{1,*} Vanja Dukic,² Jonathan Dushoff,³ Arietta Fleming-Davies,^{1,†} and Greg Dwyer^{1,‡}

1. Department of Ecology and Evolution, University of Chicago, Chicago, Illinois 60637; 2. Department of Applied Mathematics, University of Colorado, Boulder, Colorado 80309; 3. Department of Biology, McMaster University, Life Sciences 332, Hamilton, Ontario L8S 4K1, Canada

Submitted August 29, 2016; Accepted January 23, 2017; Electronically published Month XX, 2017

Online enhancements: appendixes. Dryad data: <http://dx.doi.org/10.5061/dryad.8mv03>.

q1

ABSTRACT: Eco-evolutionary theory argues that population cycles in consumer-resource interactions are partly driven by natural selection, such that changes in densities and changes in trait values are mutually reinforcing. Evidence that the theory explains cycles in nature, however, is almost nonexistent. Experimental tests of model assumptions are logically impractical for most organisms, while for others, evidence that population cycles occur in nature is lacking. For insect baculoviruses in contrast, tests of model assumptions are straightforward, and there is strong evidence that baculoviruses help drive population cycles in many insects, including the gypsy moth that we study here. We therefore used field experiments with the gypsy moth baculovirus to test two key assumptions of eco-evolutionary models of host-pathogen population cycles: that reduced host infection risk is heritable and that it is costly. Our experiments confirm both assumptions, and inserting parameters estimated from our data into eco-evolutionary insect-outbreak models gives cycles closely resembling gypsy moth outbreak cycles in North America, whereas standard models predict unrealistic stable equilibria. Our work shows that eco-evolutionary models are useful for explaining outbreaks of forest insect defoliators, while widespread observations of intense selection on defoliators in nature and of heritable and costly resistance in defoliators in the lab together suggest that eco-evolutionary dynamics may play a general role in defoliator outbreaks.

Keywords: heritability, trade-offs, host-pathogen, complex dynamics, eco-evolutionary.

Introduction

Eco-evolutionary theory has shown that natural selection can help drive cycles in predator-prey and other consumer-resource interactions, such that changes in trait values drive

changes in population densities and vice versa (Abrams 2000). Recent work has focused in particular on the case for which selection by the consumer drives selection on the resource (Ellner 2013). In this case, increases in consumer attack rates lead to both reductions in resource densities and selection-driven increases in resource resistance, while decreases in attack rates lead to both increases in resource densities and selection-driven reductions in resistance because of a fitness trade-off between resistance and fecundity. In eco-evolutionary dynamics, changes in population densities and changes in trait values are thus mutually reinforcing.

Eco-evolutionary cycles occur in predator-prey models (Abrams and Matsuda 1997; Doebeli 1997; Ellner et al. 2011; Schreiber et al. 2011), host-parasitoid models (Sasaki and Godfray 1999), and host-pathogen models (Dieckmann 2002; Elderd et al. 2008), suggesting that eco-evolutionary cycles should be widespread in nature. Moreover, laboratory microcosms have provided conclusive evidence of eco-evolutionary predator-prey cycles in real consumer-resource interactions (Fussmann et al. 2000; Yoshida et al. 2003). Field tests of the theory, however, are almost nonexistent (Abrams 2000), which is important because conditions in nature are often very different from conditions in the lab. It is thus unclear whether eco-evolutionary consumer-resource cycles occur in nature.

We therefore tested eco-evolutionary theory using field data for the gypsy moth (*Lymantria dispar*) and its baculovirus pathogen. Insect-baculovirus interactions provide useful systems for testing models of host-pathogen interactions because they can be used in field experiments designed to estimate overall infection risk (Elderd 2013), which in eco-evolutionary models is equivalent to host resistance (Dieckmann 2002). Previous studies of the heritability and costs of resistance—whether in insects (Watanabe 1987; Boots and Begon 1993; Cory and Myers 2009) or in other hosts (Altizer et al. 2003)—have in contrast relied mostly on laboratory experiments in which all hosts are forced to be exposed to the pathogen, so that the experiments measure infection risk given exposure rather than overall infection risk. Even if exposure risk is allowed to vary, host behavior in the lab-

* Present address: Department of Microbiology and Immunology, Montana State University, Bozeman, Montana 59717.

† Present address: Department of Biological Sciences, Virginia Polytechnic Institute and State University, Blacksburg, Virginia 24061.

‡ Corresponding author; e-mail: gdwyer@uchicago.edu.

ORCIDs: Dushoff, <http://orcid.org/0000-0003-0506-4794>; Dwyer, <http://orcid.org/0000-0002-7387-2075>.

Am. Nat. 2017. Vol. 189, pp. 000–000. © 2017 by The University of Chicago. 0003-0147/2017/18906-57\$15.00. All rights reserved.

DOI: 10.1086/691537

oratory may be artificially constrained in a way that substantially alters overall risk (Eakin et al. 2015). In insect-baculovirus interactions, however, it is possible to carry out field experiments that allow for natural variation in host behavior, leading to estimates of overall infection risk that match those estimated from epizootics in nature (Dwyer et al. 1997). In the first step in our research, we therefore used field experiments to test the assumptions of eco-evolutionary models that resistance is heritable and costly.

Because our experiments supported the model assumptions, in the second step in our research, we tested the model prediction that natural selection helps drive population cycles. In a few previous studies, the heritability of overall infection risk has at least been measured in the laboratory or the greenhouse (Henter and Via 1995; Herzog et al. 2007; Zbinden et al. 2008; Auld et al. 2013, 2014), but these experiments have used hosts for which there is no evidence of population cycles in nature. For the gypsy moth and other defoliating insects, however, the economic damage imposed by outbreaks has driven the collection of extensive data sets documenting population cycles (Liebhold and Kamata 2000; Johnson et al. 2005). Experimental manipulation of such cycles is impractical, because defoliator outbreak cycles occur over timescales of decades and spatial scales of thousands of square kilometers (Liebhold and Kamata 2000), but the data nevertheless allow us to indirectly test the predictions of our models. We thus tested whether our data and our models are consistent with gypsy moth cycles in nature by comparing the predictions of models parameterized from our experimental data to observational data on gypsy moth population cycles.

Previous efforts to explain gypsy moth population cycles have met with limited success. Classical insect-pathogen models require variability in host infection risk to prevent pathogen extinction, but realistically high variability causes the models to produce a stable equilibrium instead of cycles (Dwyer et al. 2000). Extending classical models to include effects of induced plant defenses on disease transmission produces models that again show realistic cycles, but these cycles require particular spatial configurations of tree species (Elder et al. 2013). Host-pathogen/induced-defense models therefore cannot explain observations of outbreaks

q2

in some forest types (Haynes et al. 2009).

Adding heritable variation in resistance to classical insect outbreak models in contrast leads to realistic cycles for realistic variability in host infection risk, irrespective of forest type (Elder et al. 2008). Moreover, baculovirus mortality is often high during gypsy moth outbreaks (Woods and Elkinton 1987), implying that selection pressure is high, while resistance in the lab is heritable and costly (Páez et al. 2015). Eco-evolutionary models may therefore provide a better explanation for gypsy moth outbreak cycles than existing models.

Previous eco-evolutionary insect outbreak models nevertheless made the unrealistic but mathematically convenient assumption that heritability is perfect (Elder et al. 2008), whereas in nature heritability is almost certainly <1 . Moreover, reduced heritability is strongly stabilizing in predator-prey models (Schreiber et al. 2011), so if the heritability of resistance to the baculovirus is too low, cycles may not occur in the models. Whether eco-evolutionary insect-outbreak models can explain gypsy moth outbreak cycles is therefore an open question.

Testing whether our experimental estimates of the heritability and cost of infection risk are consistent with gypsy moth population cycles therefore required that we extend previous eco-evolutionary insect outbreak models to allow for imperfect heritability. Because the predictions of the parameterized models match the data, we conclude that eco-evolutionary consumer-resource cycles occur in nature, not just in microcosms. Because the gypsy moth is a major pest of hardwood forests in North America (Elkinton and Liebhold 1990), and because the virus plays a role in gypsy moth control (Podgwaite et al. 1993), our models may be practically useful for guiding gypsy moth management, as we discuss.

Methods

Baculovirus Biology and Eco-Evolutionary Models of Insect Outbreaks

In defoliating insects like the gypsy moth, baculovirus transmission occurs when larvae accidentally consume foliage contaminated with infectious occlusion bodies, microscopic particles with a 10–20-nm radius that are released in large numbers (10^6 – 10^9) from the cadavers of infected conspecifics (Cory and Hoover 2006). In an occlusion body, DNA-containing virions are enclosed in a polyhedral-shaped protein matrix, which dissolves in the alkaline conditions of the insect midgut, freeing the virions so that they can infect the insect's tissues (Funk et al. 1997). Consumption of a large enough dose leads to death, after which viral enzymes break down the larval cuticle, releasing occlusion bodies into the environment to complete the cycle of transmission (Elder 2013). In high-density insect populations, multiple rounds of transmission cause severe mortality, terminating outbreaks (Moreau and Lucarotti 2007). The virus then overwinters by contaminating the egg masses produced by surviving insects, and hatching larvae become infected as they chew their way out of contaminated eggs the following spring (Murray and Elkinton 1989).

Because gypsy moths have only one generation per year, and because only larvae can become infected, there can be only one epizootic per year (Fuller et al. 2012). To model gypsy moth outbreaks, we therefore first constructed a

continuous-time epizootic submodel, which we embedded inside a discrete generation model of long-term population dynamics and evolutionary change (Elderd et al. 2008). The epizootic submodel thus uses the initial densities of hosts and pathogen particles and the initial average infection risk (as calculated by the long-term model) to calculate the fraction of hosts that become infected. The fraction infected is in turn used in the long-term model to update the number of hosts and pathogen particles and the average host infection risk. Although the model is constructed to describe gypsy moth-baculovirus interactions, it is general enough to describe many host-pathogen interactions for which hosts have discrete generations.

The epizootic submodel is a susceptible-exposed-infected-recovered (SEIR) model (Keeling and Rohani 2008), modified to allow for host variation in infection risk (Dwyer et al. 1997, 2002; Fuller et al. 2012):

$$\frac{dS}{dt} = -\bar{\nu}SP \left[\frac{S(t)}{S(0)} \right]^V, \quad (1)$$

$$\frac{dE_1}{dt} = \bar{\nu}SP \left[\frac{S(t)}{S(0)} \right]^V - m\delta E_1, \quad (2)$$

$$\frac{dE_j}{dt} = m\delta E_{j-1} - m\delta E_j, j = 2, \dots, m, \quad (3)$$

$$\frac{dP}{dt} = m\delta E_m - \mu P. \quad (4)$$

Here S and P are the densities of healthy hosts and pathogen-infected cadavers, respectively, so that I for infected host in the standard SEIR model is replaced by P for pathogen. Like most host-pathogen models, this model is fundamentally similar to Lotka-Volterra predator-prey models (Anderson and May 1992), except that host reproduction is instead described by the long-term model, as we will explain.

At field temperatures, gypsy moth larvae die an average of 16 days after consuming an infectious dose (Fleming-Davies et al. 2015), and so we allowed for a delay between infection and death. To do this, we included multiple classes of exposed but not yet infectious hosts E_j , which produces a delay between infection and death that follows a gamma distribution. To explain why multiple exposed classes produce a gamma-distributed delay, we observe that if all hosts were in class j , then the dynamics of class j would follow exponential decay $dE_j/dt = -m\delta E_j$, implying that the time spent in class j is exponentially distributed with mean $1/m\delta$. The time between infection and death is then the sum of m such exponentially distributed kill times, and a standard result from probability theory states that the sum of m exponential random variables follows a gamma distribution, in this case, with mean $1/\delta$ and coefficient of variation (CV) $1/m^{1/2}$ (Keeling and Rohani 2008).

Variation in infection risk modulates transmission through the term $\bar{\nu}[S(t)/S(0)]^V$, such that the initial mean transmission rate is $\bar{\nu}$ and the squared CV of transmission rates is V (Dwyer et al. 2000). Because $S(t) < S(0)$ for all t , higher variation V thus reduces overall transmission. To explain why this is so, we note that an increase in V without a change in $\bar{\nu}$ implies that there have been increases in the resistance of some individuals—and reductions in the resistance of others—in such a way that the mean does not change but overall variation increases. In this hypothetical situation, it is possible to show that the increases in resistance that have occurred in some individuals have bigger effects on the infection rate than do the decreases in resistance that have occurred in others (Anderson and May 1992).

The SEIR equations (1)–(4) are then used to calculate the fraction of hosts infected by the virus $i(N_n, Z_n, \bar{\nu}_n) \equiv S(T)/S(0)$, where $T = 8$ weeks is the length of the epizootic (Fuller et al. 2012). The fraction infected is in turn used in the long-term model to calculate the number of offspring produced by the surviving hosts, the number of infectious cadavers that survive the winter, and the change in infection risk that results from natural selection (for the derivation, see app. A). Because gypsy moths often experience high mortality from generalist predators and parasitoids (Gould et al. 1990; Elkinton et al. 1996), we also include a term that describes the fraction of hosts that survive predation (Dwyer et al. 2004):

$$N_{n+1} = re^{\epsilon_n} N_n [1 - i(N_n, Z_n, \bar{\nu}_n)] \left(1 - \frac{2a\omega N_n}{\omega^2 + N_n^2} \right) \\ \{1 + s\bar{\nu}_n [1 - i(N_n, Z_n, \bar{\nu}_n)]^V\}, \quad (5)$$

$$Z_{n+1} = \phi N_n i(N_n, Z_n, \bar{\nu}_n) + \gamma Z_n, \quad (6)$$

$$\bar{\nu}_{n+1} = \bar{\nu}_n [1 - i(N_n, Z_n, \bar{\nu}_n)]^{bV} \\ \frac{\{1 + s\bar{\nu}_n (bV + 1) [1 - i(N_n, Z_n, \bar{\nu}_n)]^{bV}\}}{1 + s\bar{\nu}_n [1 - i(N_n, Z_n, \bar{\nu}_n)]^{bV}}. \quad (7)$$

Host density N_{n+1} is the product of baseline fecundity r , a stochasticity term e^{ϵ_n} , host density in the preceding generation N_n , and the fraction surviving the epizootic $1 - i(N_n, Z_n, \bar{\nu}_n)$. The stochasticity parameter ϵ_n is a normal random variate with mean 0 and standard deviation σ , representing the stochastic effects of weather (Williams et al. 1990). Generalist predation is represented by the term $1 - 2a\omega N_n / (\omega^2 + N_n^2)$, which describes host survival as determined by a type III functional response (Dwyer et al. 2004). To allow for the cost of resistance, we assume that fecundity at low host and pathogen densities increases linearly with increasing infection risk $\bar{\nu}_n$, according to $1 + s\bar{\nu}_n [1 - i(N_n, Z_n, \bar{\nu}_n)]$. Changes in host density are thus partly driven by balancing

selection, such that higher average infection risk \bar{v}_n leads to increased mortality but also to increased fecundity. The fecundity cost of resistance is reduced, however, when the infection rate $i(N_n, Z_n, \bar{v}_n)$ is high, which is more likely when average infection risk is high or when host and pathogen densities are high. Increases in average infection risk or in host and pathogen densities thus reduce the fecundity cost but also increase host mortality.

Pathogen density Z_{n+1} is equal to the density of infectious cadavers produced in the preceding generation's epizootic, $N_n i(N_n, Z_n, \bar{v}_n)$, times the effective overwintering rate ϕ . We refer to ϕ as the effective overwintering rate because it allows for both pathogen survival and the higher susceptibility of neonate larvae (Dwyer et al. 2000). Because neonates are orders of magnitude more susceptible than later-stage larvae, previous work has shown that $\phi > 1$ (Fuller et al. 2012; Fleming-Davies and Dwyer 2015). Longer-term pathogen survival is represented by the cadaver density Z_n times the long-term pathogen survival rate γ (Fuller et al. 2012).

Infection risk \bar{v}_{n+1} is equal to the preceding generation's infection risk \bar{v}_n times the fraction infected $i(N_n, Z_n, \bar{v}_n)$, so that higher virus mortality selects for reduced risk. The cost of resistance in contrast selects for higher risk, because fecundity at low densities increases linearly with increases in previous-generation risk, $1 + s\bar{v}_n(bV + 1)[1 - i(N_n, Z_n, \bar{v}_n)]^{bV}$, an effect that is again reduced by high infection rates. The symbol b represents the heritability of risk, so that bV is the fraction of overall variation in risk that is due to additive genetic factors, and high values of b strengthen the effects of selection. Changes in infection risk are thus determined by balancing selection, as in the case of host density, except that in contrast to host density, the change in infection risk does not depend on the baseline fecundity r .

Population cycles in this model then occur because of the consumer-resource interaction between the host and the pathogen and because of natural selection on infection risk and fecundity (fig. 1). Low virus mortality drives increases in the density of high-fecundity, high-infection-risk genotypes, leading to increases in the density of the virus and increases in the average infection risk, which in turn cause virus epizootics that decimate the host population. Host density is then low for multiple host generations not just because of the pathogen and the generalist predators but also because the survivors of virus epizootics are more resistant to the pathogen and therefore have low fecundity. Eventually, however, reductions in the density of the virus and increases in the fecundity of the insect drive increases in the density of the host, leading to a new outbreak. Natural selection therefore combines with ecological factors to drive outbreaks. Qualitatively similar behavior occurs in models in which there is no generalist predator or in which the pathogen is replaced by a parasitoid (see app. B, available online).

Field Experiments to Estimate the Heritability and Cost of Reduced Infection Risk

Our experiments were designed to test the two key assumptions of our eco-evolutionary model: that infection risk is heritable and that there is a fecundity cost of reduced risk. Previous work produced preliminary evidence that infection risk is heritable without estimating heritability and without showing that there is a cost of reduced risk (Elder et al. 2008). In testing whether infection risk is heritable and costly, we therefore also aimed to estimate the heritability parameter b and the cost parameters r and s to determine whether the values of these parameters fall in the right range to produce realistic model outbreaks. To estimate b , we carried out a field transmission experiment using half-sibling families, which we created by taking advantage of the ability of male gypsy moths to mate with two to three different females, given 24 h of rest between matings (Páez et al. 2015). To estimate r and s , we carried out a field transmission experiment using full-sibling families, which we produced by mating individual males to individual females.

We carried out our experiments in the field because overall infection risk depends on feeding behavior, which cannot be easily allowed for in laboratory experiments (Dwyer et al. 2005). Feeding behavior affects overall risk by determining exposure risk (Eakin et al. 2015), but overall risk is also affected by risk given exposure, which is instead determined by the insect's immune system (Páez et al. 2015). Moreover, in the lab, both feeding behavior and immune system functioning show heritable variation that affects exposure risk and infection risk given exposure, respectively (Parker et al. 2011; Páez et al. 2015). By measuring overall infection risk, we thus allowed for heritable variation in both feeding behavior and immune system functioning. In previous work, inserting estimates of infection risk from this type of experiment into the SEIR equations (1)–(4) produced infection rates close to those seen in nature (Dwyer et al. 1997, 2002), suggesting that our experimental protocol allows for accurate estimation of infection risk.

Estimating the heritability of infection risk then required that we decompose the variance in risk into additive genetic variance and environmental variance (Falconer and Mackay 1996). Additive genetic variance can be estimated from the variance across half-sibling groups, which is due to sire effects S_i , while environmental variance instead arises from maternal effects M_j because of variability in egg provisioning (Diss et al. 1996) or small-scale differences between rearing cups. Also, for logistic reasons, larvae were not all deployed in the field on the same day, and so environmental variance may also arise from a start-day effect D_k .

Because infection risk is defined in equations (1)–(4) as the transmission rate \bar{v} , we first expressed \bar{v} in terms of sire, dam, and day effects:

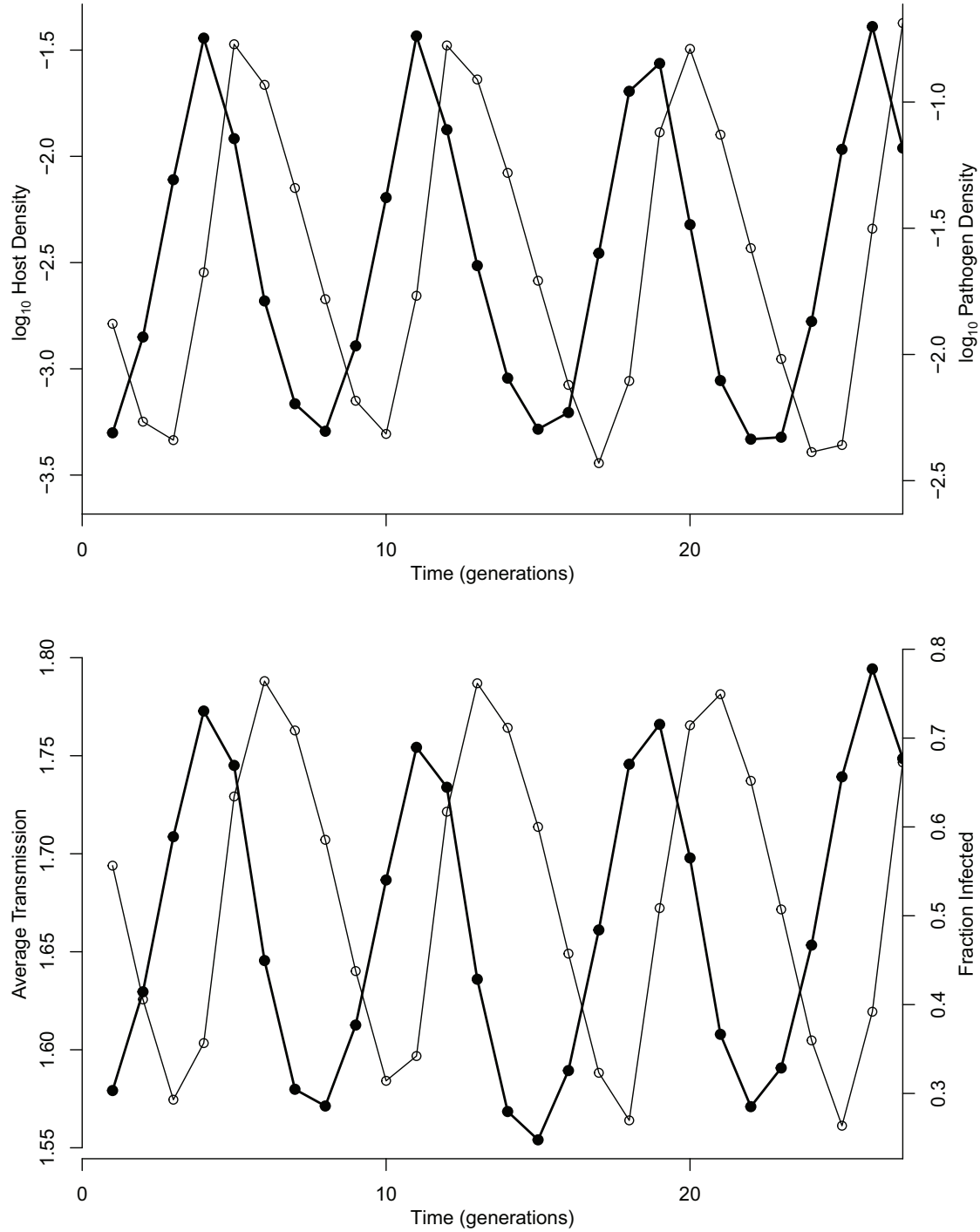


Figure 1: Single realization of the model equations (5)–(7). Top panel shows changes in host N_n (filled circles, black lines) and pathogen Z_n (open circles, gray lines) densities, while bottom panel shows changes in average infection risk \bar{v}_n (filled circles, black lines) and in the fraction infected i (open circles, gray lines). Here we use the median parameters calculated from our experimental data: heritability $b = 0.129$, baseline fecundity $r = 0.21$, cost-scaling parameter $s = 1.21$, and total variation $V = 2.97$. The death rate of exposed hosts $\delta = 1/16$ per day and the number of classes $m = 27$ are from Fleming-Davies et al. (2015). The generalist predation parameters $a = 0.96$ and $w = 0.14$ are from Dwyer et al. (2004). The pathogen overwintering parameter $\phi = 7.4$ and the long-term survival parameter $\gamma = 0.3$ are from Fuller et al. (2012). Long-term survival γ is on the high end of reasonable values, but variation in γ has only modest effects (app. B, available online).

$$\bar{v}_{jkl} = e^{\log(v^*) + S_j + M_k + D_l}. \quad (8)$$

Here v^* is the baseline infection risk. A basic result from quantitative genetic theory (Falconer and Mackay 1996) then states that heritability can be expressed in terms of the sire variance σ_s^2 , the maternal variance σ_M^2 , and the day variance σ_D^2 :

$$b = 4 \times \frac{\sigma_s^2}{(\sigma_s^2 + \sigma_M^2 + \sigma_D^2)}. \quad (9)$$

Estimating σ_s^2 , σ_M^2 , and σ_D^2 then required that we relate infection risk \bar{v}_{jkl} to a measurable quantity. To do this, we used \bar{v}_{jkl} in the SEIR equations (1)–(4) to calculate the fraction infected, as measured in our experiments. In practice, we first simplified the SEIR equations, because in our experiments, the mesh bags block enough sunlight that decay is 0 (Fuller et al. 2012) and the exposure period is short enough (7 days) that no new virus deaths occur. These two factors ensure that the density of virus does not change during the experiments, so that we can set $dP/dt \equiv 0$ in equations (1)–(4), which in turn allows us to derive an expression for the fraction infected i in terms of \bar{v}_{jkl} (Dwyer et al. 2000):

$$i = 1 - [1 + \bar{v}_{jkl} VP(0)T]^{-1/V}. \quad (10)$$

Here $P(0)$ is the density of virus-infected cadavers and T is the length of time for which the experiment runs. Because in our experiments we varied the density of virus-infected cadavers, we were able to fit \bar{v}_{jkl} and V to our data, which made it possible to estimate the effects of sire, dam, and day on infection risk. To do this, we used a hierarchical Bayesian fitting routine (see app. B), such that the sire, maternal, and day effects were drawn from normal distributions with mean 0 and respective variances σ_s^2 , σ_M^2 , and σ_D^2 . Once we had estimates of σ_s^2 , σ_M^2 , and σ_D^2 , we inserted them into equation (9) to estimate the heritability b of infection risk. We also tested more directly whether there was meaningful heritable variation by using Akaike information criterion (AIC) analysis to choose between models that included sire, dam, and day effects in different combinations.

Inferences about transmission parameters are stronger in experiments that include a range of virus densities (Elderd et al. 2008), and so we used densities of 0, 25, 50, and 75 virus-infected cadavers per 40-leaf branch. Each branch was fed on by roughly 20 uninfected larvae, a density that falls within the range of gypsy moth densities observed at the start of baculovirus epizootics (Woods and Elkinton 1987). After larvae had fed freely on virus-contaminated foliage in the field, we reared them in individual diet cups in the lab until death or pupation. Infected larvae are usually easily recognizable because the virus has caused them to disintegrate, but in cases of uncertainty, we examined smears from dead larvae under a light microscope for the presence of occlusion bodies, which are easily visible at  0 (Woods and Elkinton 1987).

Because we used an area in which gypsy moth densities were very low, and because all eggs were surface sterilized in dilute formalin (Dwyer and Elkinton 1995), infection rates on uninfected control foliage were low (heritability experiment: 12/209 = 5.7%; cost experiment: 6/371 = 1.6%), and so we do not consider controls further.

In our fitting routine, we assumed that the data are binomially distributed, which is equivalent to assuming that infection risk is independent across larvae within a branch, but in practice there may be correlations in infection risk between larvae that cause the observed variance to be higher than the binomial variance (McCullagh and Nelder 1989; see app. B; note that this is a nonissue for our analyses of the cost of resistance data, which instead rely on bootstrapping to quantify uncertainty). A standard way to test for such extrabinomial variation is to calculate the variance inflation factor, the ratio of the observed variance to what the corresponding binomial variance would be, given the sample size (Burnham and Anderson 2002). Variance inflation factors >4 suggest that there is substantial model inadequacy, but smaller values can instead be used to adjust the likelihood score, leading to a quasi-likelihood AIC (QAIC). In our experiments, we kept extrabinomial variation reasonably low by ensuring that all uninfected larvae had reached the fourth instar within 48 h of the beginning of the experiment (Elderd et al. 2008; see app. B), leading to a variance inflation factor of 2.27. We then divided the likelihood score of each model by 2.27 before calculating AIC values, thus using QAIC scores to choose the best model (Burnham and Anderson 2002).

In principle, sire, dam, and day effects could explain all the variation in infection risk so that we could allow $V \rightarrow 0$ in equation (10) (Dwyer et al. 2005), but there are also effects of small-scale spatial variation in virus density that do not depend on factors that vary between host families (Eakin et al. 2015). Because of this variation, allowing $V \rightarrow 0$ in equation (10) produced a model that gave a much worse fit to the data, and we therefore instead assumed $V > 0$.

To estimate the cost of reduced infection risk, we fit a version of the fraction-infected equation (10) to the data for each full-sibling group, and we regressed average female pupal weight in each group on the average infection risk in that group (Elderd et al. 2008). Because pupal weight is a good predictor of egg number (Páez et al. 2015; $r^2 = 0.57$), a positive relationship between pupal weight and infection risk indicates that there is a fecundity cost of reduced risk. Because we measured fecundity in terms of pupal weight, however, estimating the cost parameters r and s required that we convert from pupal weight to egg number. We did this in two steps: first, by using data from Páez et al. (2015) to convert from pupal weight to egg mass weight, and second, by using data from Dwyer and Elkinton (1995) to convert from egg mass weight to egg number. An additional consideration, however, is that the model requires an estimate of net fecundity,

because early instars often die from starvation as they disperse from egg masses laid on bark to foliage at branch tips. To allow for such losses, we used data from Hunter and Elkinton (2000), who measured early instar survival in experimental gypsy moth populations. We then bootstrapped to estimate the net uncertainty arising from the three conversions (app. B).

Results

In the heritability experiment, infection rates and infection risk varied strongly across half-sibling families (fig. 2A, 2B), with 13% of the variation in risk explained by additive genetic variation ($b = 0.13$). QAIC scores were vastly better (lower) for models with sire effects (table 1), while the model with sire and dam effects was the only model with a substantial QAIC weight, indicating that dam effects were also strong but that day effects were weak. Because the models include random effects, it is almost impossible to assess goodness of fit through visual inspection of plots of the model predictions and the data versus virus densities, as is usually done with this kind of experiment (Elder 2013), but in appendix B, we use a plot of observed versus predicted infection rates to demonstrate that the best model is quite accurate. For heritability b , the 95% highest posterior density (HPD) interval (the Bayesian equivalent of a 95% confidence interval) was broad but excluded values below 5×10^{-4} (HPD = 0.0005, 0.51). Infection risk in the gypsy moth therefore has low but nonzero heritability, confirming the first key assumption of our eco-evolutionary model.

In the cost experiment, there was a noisy but positive relationship between female pupal weight and infection risk (fig. 2C), and the slope of the regression line was significantly >0 , confirming that there is a cost of reduced risk (median intercept = 0.73, upper and lower 95th percentiles = 0.70, 0.80; median slope = 0.45, upper and lower 95th percentiles = 0.09, 0.56; for a description of how we bootstrapped the regression parameters to account for error in both infection risk and pupal weight, see app. B). In this regression, we included only survivors of virus exposure, which may have led to an underestimate of the cost, because of selection for low-risk/low-fecundity individuals within full-sibling groups. We therefore carried out a second regression (see app. B) in which we also included unexposed larvae from the lab, but the resulting regression line had identical slopes for exposed and unexposed individuals (intercepts in contrast were different, probably because lab-reared insects have artificially high growth (Páez et al. 2015); thus, in estimating costs, we used weights for field-reared insects. Irrespective of the analysis, our data show that female gypsy moths experience a fecundity cost of reduced infection risk, confirming the second key assumption of our eco-evolutionary model.

Because infection risk is heritable and costly, balancing selection must inevitably play a role in determining infection risk in the gypsy moth. It does not follow, however, that selection alters gypsy moth outbreak cycles, because realistic cycles in our model do not occur for all parameter values. To test whether our experimental parameters give realistic cycles, we therefore simulated the model using the experimental parameters to determine whether the parameterized model can reproduce data on gypsy moth outbreak cycles.

Because cyclic population dynamics are at least moderately sensitive to initial densities, which are almost always unknown, Kendall et al. (1999) argued that a useful way to compare model cycles to data is by comparing periods and amplitudes, which in the long run are insensitive to initial conditions. Accordingly, when we inserted the median parameter values calculated from our experiments into our model, the average cycle period was 7.4 years, and the average amplitude was 2.1 orders of magnitude (fig. 1), which compares well with observed periods of 5–9 years (Johnson et al. 2005) and observed amplitudes of 2–4 orders of magnitude (Skaller 1985; Williams et al. 1990; Jones et al. 1998). Moreover, variation in the parameter estimates has only modest effects on model periods and amplitudes (fig. 3). Finally, the model predicts that average infection risk (fig. 1) will fall in synchrony with falling population densities, a prediction that was confirmed by previous experiments that measured infection risk before and after a population crash (Elder et al. 2008). Observational and experimental data thus support the model predictions, suggesting that natural selection plays an important role in gypsy moth outbreaks.

We also used our models to address the general issue of how heritability affects population stability. In continuous-time eco-evolutionary predator-prey models, stability is more likely when heritability is low (Schreiber et al. 2011), but in our model, stability is more likely when heritability is intermediate (fig. 3). In both types of models, high heritability causes such a rapid response to selection that risk undergoes large-amplitude fluctuations, driving large-amplitude fluctuations in densities. In our model, however, low heritability causes a slow response to selection that exacerbates the delayed density dependence that drives cycles, and so low heritability is mildly destabilizing instead of stabilizing. This destabilizing effect of low heritability also occurs in a model in which the pathogen is replaced by a parasitoid (see app. B), but the effect almost disappears in a model in which the epizootic continues until it has burned out as a result of low densities of susceptible hosts (Dwyer et al. 2000; see app. B).

The lack of a destabilizing effect in the burnout model is likely due to the less severe effects of delayed density dependence in that model. That is, when the epizootic proceeds to burnout, the pathogen responds more rapidly to density, reducing the delay between increases in host density and

q3 

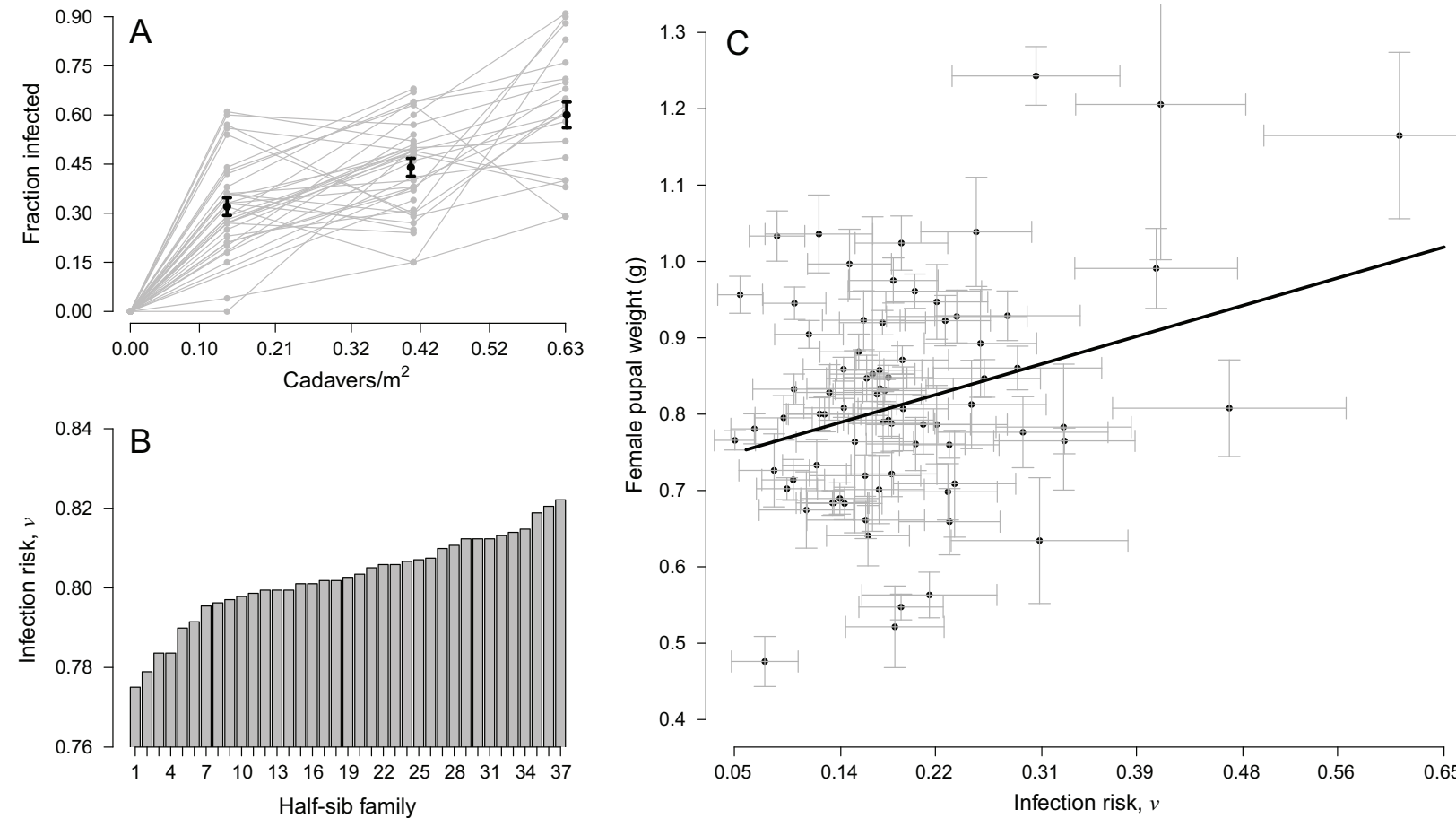


Figure 2: A, Relationship between fraction infected and density of virus-infected cadavers in our heritability experiment. Gray lines show the data for each half-sibling family, while black circles show the average and 1 SE of the mean (table 1). Median values for $\bar{\nu}$ and V are 0.80 (highest posterior density [HPD] interval = 0.43, 1.37) and 2.97 (HPD = 1.55, 4.59), respectively, which are close to values from previous experiments (Elderd et al. 2008). B, Variation in average infection risk $\bar{\nu}$ across half-sibling families, again suggesting that infection risk is heritable. C, Fecundity cost of resistance, as demonstrated by a positive relationship between infection risk and female pupal mass, a proxy for fecundity (Páez et al. 2015). Data underlying this figure are deposited in the Dryad Digital Repository: <http://dx.doi.org/10.5061/dryad.8mv03> (Páez et al. 2017).

Table 1: Quasi-likelihood Akaike information criterion (QAIC) scores for transmission models

Model	Parameters	No. parameters	QAIC	weight
1	$\nu, V, \text{sire}_b, \text{dam}_j, \text{day}_k$	131	2.83	.06
2	$\nu, V, \text{dam}_j, \text{day}_k$	93	89.4	$<10^{-5}$
3	$\nu, V, \text{sire}_b, \text{dam}_j$	124	0	.944
4	ν, V, sire_i	40	14.6	$<10^{-5}$

Note: Boldface indicates the best model, which allows for sire and dam effects.

increases in pathogen density, in turn reducing the period and amplitude of outbreak cycles. Discrete generations nevertheless also appear to play a role, in that stability in the burnout model is at least slightly lower at low heritability. We therefore conclude that the effects of heritability on stability are modulated by the severity of the delayed density dependence, which in turn depends on the occurrence of discrete generations.

A second general point is that our model does not appear to have either the half-cycle lags (Yoshida et al. 2003) nor the cryptic population cycles (Yoshida et al. 2007) that have been observed in microcosm models. We have not been able to prove this result, but for almost all the parameter values in figure 3, the average lag was two generations or less (99.6% of 96,981 parameter sets that did not cause host or pathogen extinction), strongly suggesting that longer lags do not occur. Meanwhile, in outbreak data on several different insects, baculovirus infection rates likewise peaked shortly after host densities (Moreau and Lucarotti 2007), confirming the model prediction.

A full understanding of why our model behaves differently from microcosm models is beyond the scope of our work. We note, however, that half-cycle lags in microcosm models are more likely when costs are low, whereas in our model, reducing the cost-scaling parameter s had no effect on the lag (for $s = 0.2$, the lower bound on the HPD: 94.8% of 87,515 parameter sets had lags of two generations or less; for $s = 0.2$: 91.3% of 13,387 parameter sets; note that reducing s tends to increase the probability of host and/or pathogen extinction; see app. B). The key difference between our model and microcosm models therefore again appears to be that our model assumes discrete host generations, whereas microcosm models assume continuous reproduction (Hiltunen et al. 2014).

Discussion

In comparing the cycles in our models to cycles in North American gypsy moth populations, it is important to point out that Allstadt et al. (2013) showed that gypsy moth pop-

ulations in New England cycled from 1943 to 1965 and from 1978 to 1996, with periods of noncyclic dynamics at other times (data points after 2009 were too few to permit testing, but a 2016 outbreak in New England suggests that cycling may have returned; G. Dwyer, personal observation). This lack of cycling is not necessarily inconsistent with our models, however, because Allstadt et al. showed that the dynamics seen in the New England data can be explained by a version of the Dwyer et al. (2004) model that includes stochastic fluctuations in generalist-predator density. Given that our model is basically the Dwyer et al. model plus natural selection, it seems likely that adding stochastic fluctuations in generalist-predator density to our model would allow it to reproduce the New England data, with the proviso that such a test is beyond the scope of our work.

Another important feature of Allstadt et al.'s work, however, is that they forced their version of the nonevolutionary Dwyer et al. model to show at least intermittent cycles, by using values of host variation V that are now known to

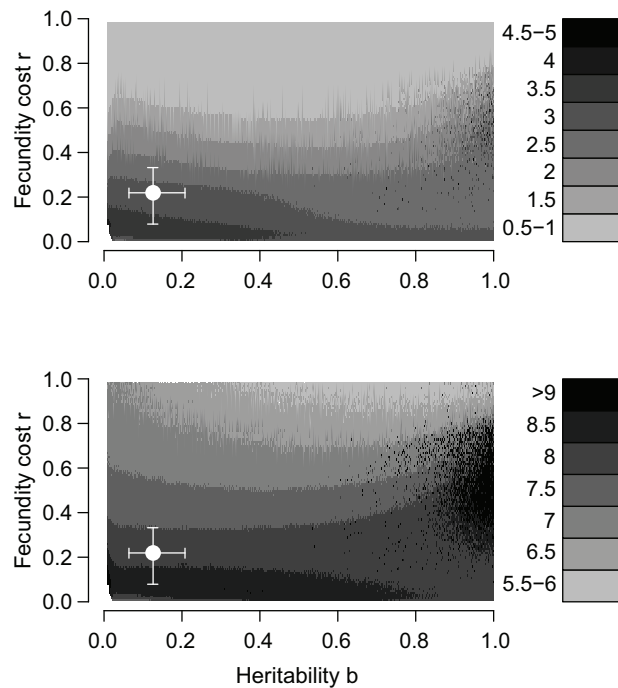


Figure 3: Effects of variation in baseline fecundity r and heritability b on the period and amplitude of outbreak cycles in the long-term model (eqq. [5]–[7]). Here and in similar figures in appendix B (available online), each period and amplitude is an average over 25 realizations of the model. Remaining parameters are as in figure 1. Top panel shows the average cycle amplitude in orders of magnitude, while bottom panel shows the average period in years. White circle represents our median estimates of r and b , with error bars indicating the interquartile range. Because cycle periods are generally shorter and amplitudes are generally lower at intermediate values of b , we conclude that intermediate heritability is stabilizing.

be unrealistically low (Elder et al. 2008). As we have described, realistic values of V eliminate cycles altogether in nonevolutionary insect-outbreak models, leading instead to a stable, point equilibrium. Given that Allstadt et al.'s approach has been followed in several other articles (Haynes

q4  et al. 2009; Bjørnstad et al. 2010; Walter et al. 2015), a consideration of eco-evolutionary dynamics may have broad implications for our understanding of gypsy moth dynamics.

In focusing on the effects of natural selection, we nevertheless neglected other mechanisms known to affect gypsy moth outbreak cycles in North America. First, since 1989, the fungal pathogen *Entomophaga maimaiga* has often caused high mortality in North American gypsy moth populations when rainfall is high (Hajek 1999; Liebhold et al. 2013; Hajek et al. 2015). Indeed, the advent of *E. maimaiga* may provide an alternative explanation for the lack of outbreaks in New England since 1996 (Allstadt et al. 2013).

Second, we assumed that baculovirus transmission is unaffected by host-plant foliage quality, but defoliation-induced increases in hydrolyzable tannins in oaks (*Quercus* spp.) can greatly reduce variation in infection risk. Because of this effect, host-pathogen/induced-defense models can help explain variability in outbreak periods across forest types (Elder et al. 2013). Although the models do not allow for outbreaks in forest types with low frequencies of oaks, where outbreaks

q5  have in fact been observed (Haynes et al. 2009), and although the models are sensitive to the degree of clumping of oaks within the forest (Elder et al. 2013), which has not been measured, it nevertheless seems likely that induced defenses also affect gypsy moth outbreaks.

Third, our models assume that the pathogen population is monomorphic, but the gypsy moth virus is at least moderately polymorphic and is also subject to trade-offs between fitness components (Fleming-Davies et al. 2015). Indeed, natural selection on the pathogen is perhaps the most important missing mechanism in our model, because it is most likely to lead to changes in dynamics (Dieckmann 2002), but allowing for pathogen evolution would require extensive experiments to estimate how host trade-offs vary with pathogen strain and how pathogen trade-offs vary with host family (Hudson et al. 2016). Simple coevolutionary host-parasitoid models have nevertheless shown that coevolutionary dynamics can also help drive insect outbreak cycles while also helping to maintain variation in the host (Sasaki and Godfray 1999), which in our models is assumed constant.

Allowing for these complications is an important next step in our work, but the evidence that we have provided for the effects of natural selection suggests that selection has at least some effect on outbreaks, confirming eco-evolutionary theory in a broader sense. Nevertheless, in the absence of outbreak-scale experiments, our work cannot provide conclusive proof of eco-evolutionary cycles, a problem that afflicts most studies of complex population dynamics (Turchin 2003). For eco-

evolutionary models in particular, simultaneous collection of phenotypic and density data could provide additional evidence, but for now the combination of experimental and observational data that we have used here may provide the best support for eco-evolutionary theory.

The insect ecology literature suggests that eco-evolutionary dynamics may also play a role in population cycles of other forest defoliating insects (Anderson and May 1981; Myers 1988, 1993). First, laboratory observations of heritable variation and costs of resistance are common in insect host-pathogen (Watanabe 1987; Boots and Begon 1993; Cory and Myers 2009) and host-parasitoid (Kraaijeveld et al. 2002) interactions. Although lab experiments are limited to measurements of risk given exposure, as we described, the results of our gypsy moth field experiments qualitatively match the results of gypsy moth lab experiments (Páez et al. 2015). The large number of previous lab studies showing heritable variation in insect host-pathogen and host-parasitoid interactions therefore suggests that the effects of natural selection are widespread. Meanwhile, mortality due to baculoviruses and parasitoids is high in most cycling forest defoliators (Nealis 1991; Turchin 2003; Moreau and Lucarotti 2007), suggesting that selection pressure is often high enough to affect outbreak cycles. More broadly, because seasonality plays a role in many other host-pathogen interactions (Altizer et al. 2006), the effects of seasonal breeding in our models may be of general applicability, while the lack of half-cycle lags in our models means that a lack of such lags in general does not rule out eco-evolutionary cycles.

Baculoviruses are used as environmentally benign insecticides (Hunter-Fujita et al. 1998), which in the gypsy moth consists of the Gypchek spray product (Podgwaite et al. 1992). As is often the case with baculoviruses used in pest control, Gypchek plays only a modest role in gypsy moth control, because production costs are lower for the insecticide Btk, a naturally occurring bacterial toxin. Btk targets effectively all Lepidoptera, however, and so concerns over its environmental costs have led to increasing public demand for Gypchek (Boulton and Otvos 2004; Narciso 2014; Nolan 2015). Baculovirus spray products like Gypchek may therefore be used repeatedly in the future, and the resulting increases in infection rates may substantially alter insect outbreak cycles.

Reilly and Elder (2014) tested this hypothesis by modifying the Dwyer et al. (2004) model to allow for repeated spraying, which showed that spraying dampens population cycles, effectively eliminating outbreaks. Our eco-evolutionary models, however, show that realistic outbreaks occur in nature for a broader range of parameters than in the Dwyer et al. model, and it may therefore be the case that resistance evolution will prevent the cycle-dampening effects of repeated baculovirus sprays, with the proviso that the evolution of increased resistance will likely raise average host densities. Extending our

models to allow for repeated baculovirus sprays may thus provide a better understanding of baculovirus use in pest control, and carrying out such an extension is therefore another next step. Our models thus support the growing consensus that eco-evolutionary theory has direct relevance for applied ecology (Menalled et al. 2016; Rozins and Day 2016).

Acknowledgments

Our work was funded by National Institutes of Health grant R01GM96655 awarded to G.D., V.D., and B. J. Rehill. Research was conducted under U.S. Department of Agriculture Animal and Plant Health Inspection Service permit P526P-12-01466 to G.D. We thank J. Armagost, P. Brandt, S. Carpenter, C. Gilroy, D. Howard, C. Maguire, T. O'Halloran, Y. Ren, A. Saad, K. Smith, K. Vavra-Musser, K. Sirianni, and S. Xie for laboratory and field assistance. We thank V. Andreasen and S. Ellner for discussing our results.

APPENDIX A

Derivation of the Eco-Evolutionary Host-Pathogen Model

Elderd et al. (2013) present a version of the Dwyer et al. (2004) model that also includes heritable changes in average infection risk and a trade-off between infection risk and fecundity. Their model, however, assumes that the phenotypic and genotypic distributions of infection risk are identical, as though heritability $b = 1$. Here we instead assume that $b < 1$, which significantly complicates the derivation of the model.

The initial steps in the Elderd et al. derivation are nevertheless useful. First, the pathogen equation (6) is unchanged from the original non-evolutionary insect-pathogen model of Dwyer et al. (2000), and therefore we do not consider it here. Second, by temporarily neglecting predation, we can integrate over the phenotypic distribution to derive an equation for the host population:

$$N_{n+1} = \int (r + rsv)f_p(v)S(T)dv. \quad (A1)$$

Here $f_p(v)$ is the distribution of infection risk phenotypes v and $S(T)$ is the host density, where both are calculated after an epizootic that lasts T days. Host density is then calculated by allowing for disease-driven mortality (which determines the host density after the epizootic) and by including a fecundity cost of reproduction, as determined by the cost parameters r and s . Meanwhile, Elderd et al. assumed that $T \rightarrow \infty$, and they used the alternative parameterization $r + \lambda v$ to describe the cost function, but the effects of these differences are minor compared the complications that arise from assuming that $b < 1$.



We further follow the Elderd et al. derivation in assuming that the epizootic reduces the mean of the distribution of phenotypes but does not change the shape of the distribution, so that the squared coefficient of variation (CV) V is constant. Given this constant-shape assumption, it is possible to show that the postepizootic mean is $\bar{v}_n[S(T)/S(0)]^V$, where \bar{v}_n is the pre-epizootic mean (Dwyer et al. 2000). This assumption is also fundamental to the derivation of the susceptible-exposed-infected-recovered (SEIR) epizootic model (eqq. [1]–[4]), which is an approximation of a model that describes the entire distribution of phenotypes. The SEIR equations provide a highly accurate approximation of the full model if phenotypes follow a gamma distribution, but they are only moderately inaccurate for distributions with longer tails, such as a log-normal distribution. More importantly, for our purposes, the approximation means that both the SEIR model and the multigeneration model derived here can be simulated with only modest computational costs.

Continuing to follow the Elderd et al. derivation, we observe that the postepizootic host density is

$$S(T) = N_n[1 - i(N_n, Z_n, \bar{v}_n)], \quad (A2)$$

where $i(N_n, Z_n, \bar{v}_n)$ is calculated using equations (1)–(4). Including predation and stochasticity then gives equation (5), which is effectively the same as the host-density equation in the Elderd et al. model.

As we described, however, a crucial difference from the Elderd et al. model is that we allow the genotypic and phenotypic distributions to have different shape parameters V , which is necessary to allow for imperfect heritability. This assumption becomes important when we calculate how the average phenotype \bar{v}_n changes as a result of mating, because in calculating the change in the phenotype, we average the fecundity costs over the genotypic distribution, whereas in the host density equation (1), we average over the phenotypic distribution. Specifically, we assume that the squared CV of the genotypic distribution is bV , where V is the squared CV of the phenotypic distribution and b is the heritability. Although other assumptions may also produce a reasonably simple model, this assumption has several advantages: (1) it ensures that genotypic variation is lower than phenotypic variation, as expected from quantitative genetic theory (Falconer and Mackay 1996); (2) it is consistent with previous approaches to adding quantitative genetic variation to predator-prey models (Abrams and Matsuda 1997); and (3) it produces a model that makes intuitive sense, as we now show.

To integrate over the genotypic distribution, we proceed as follows:

$$\bar{v}_{n+1} = \frac{\int v(r + rsv)f_G(v)S(T)dv}{\int (r + rsv)f_G(v)S(T)dv}. \quad (A3)$$

Here $f_G(\nu)$ is the postepizootic distribution of genotypes ν , and $S(T)$ is again the host density after an epidemic that lasts T days. To solve the integral, we again use the observation that the mean of the phenotypic distribution after the epizootic is $\bar{\nu}_n[S(T)/S(0)]^V$. Also, we use the assumption that the genotypic distribution has the same mean as the phenotypic distribution but that it has a squared CV equal to bV , with the proviso that for the genotypic distribution, the mean depends on the squared genotypic CV, not the phenotypic CV as in the host-density equation (A1). We then have equation (7), which we repeat here for convenience:

$$\bar{\nu}_{n+1} = \bar{\nu}_n [1 - i(N_n, Z_n, \bar{\nu}_n)]^{bV} \frac{[1 + s\bar{\nu}_n(bV + 1)[1 - i(N_n, Z_n, \bar{\nu}_n)]^{bV}]^V}{1 + s\bar{\nu}_n[1 - i(N_n, Z_n, \bar{\nu}_n)]^{bV}}. \quad (\text{A4})$$

This model makes intuitive sense, in that setting $b = 1$ again produces the Elderd et al. model, while setting $b = 0$ gives the classical model with no natural selection, as in Dwyer et al. (2000) and Dwyer et al. (2004).

Literature Cited

- Abrams, P. 2000. The evolution of predator-prey interactions: theory and evidence. *Annual Review of Ecology and Systematics* 31:79–105.
- Abrams, P. A., and H. Matsuda. 1997. Prey adaptation as a cause of predator-prey cycles. *Evolution* 51:1742–1750.
- Allstadt, A. J., K. J. Haynes, A. M. Liebhold, and D. M. Johnson. 2013. Long-term shifts in the cyclicity of outbreaks of a forest-defoliating insect. *Oecologia (Berlin)* 172:141–151.
- Altizer, S., A. Dobson, P. Hosseini, P. Hudson, M. Pascual, and P. Rohani. 2006. Seasonality and the dynamics of infectious diseases. *Ecology Letters* 9:467–484.
- Altizer, S., D. Harvell, and E. Friedle. 2003. Rapid evolutionary dynamics and disease threats to biodiversity. *Trends in Ecology & Evolution* 18:589–596.
- Anderson, R. M., and R. M. May. 1981. The population dynamics of micro-parasites and their invertebrate hosts. *Philosophical Transactions of the Royal Society B* 291:451–524.
- . 1992. Infectious diseases of humans: dynamics and control. Oxford University Press, Oxford.
- Auld, S. K. J. R., S. R. Hall, J. H. Ochs, M. Sebastian, and M. A. Duffy. 2014. Predators and patterns of within-host growth can mediate both among-host competition and evolution of transmission potential of parasites. *American Naturalist* 184(suppl.):S77–S90.
- Auld, S. K. J. R., R. M. Penczykowski, J. H. Ochs, D. C. Grippi, S. R. Hall, and M. A. Duffy. 2013. Variation in costs of parasite resistance among natural host populations. *Journal of Evolutionary Biology* 26:2479–2486.
- Bjørnstad, O. N., C. Robinet, and A. M. Liebhold. 2010. Geographic variation in North American gypsy moth cycles: subharmonics, generalist predators, and spatial coupling. *Ecology* 91:106–118.
- Bolker, B. M. 2008. Ecological models and data in R. Princeton University Press, Princeton, NJ.
- Boots, M., and M. Begon. 1993. Trade-offs with resistance to a granulosis virus in the Indian meal moth examined by a laboratory evolution experiment. *Functional Ecology* 7:528–534.
- Boulton, T., and I. Otvos. 2004. Monitoring native non-target Lepidoptera for three years following a high dose and volume application of *Bacillus thuringiensis* subsp. *kurstaki*. *International Journal of Pest Management* 50:297–305.
- Burnham, K. P., and D. R. Anderson. 2002. Model selection and multi-model inference: a practical information-theoretic approach. 2nd ed. Springer, New York.
- Cory, J. S., and K. Hoover. 2006. Plant-mediated effects in insect-pathogen interactions. *Trends in Ecology and Evolution* 21:278–286.
- Cory, J. S., and J. H. Myers. 2009. Within and between population variation in disease resistance in cyclic populations of western tent caterpillars: a test of the disease defence hypothesis. *Journal of Animal Ecology* 78:646–655.
- Dieckmann, U. 2002. Adaptive dynamics of pathogen-host interactions. Pages 39–59 in U. Dieckmann, K. Sigmund, and H. Metz, eds. *Adaptive dynamics of infectious diseases: in pursuit of virulence management*. Cambridge University Press, Cambridge.
- Diss, A., J. Kunkel, M. Montgomery, and D. Leonard. 1996. Effects of maternal nutrition and egg provisioning on parameters of larval hatch, survival and dispersal in the gypsy moth, *Lymantria dispar*. *Oecologia (Berlin)* 106:470–477.
- Doebeli, M. 1997. Genetic variation and persistence of predator-prey interactions in the Nicholson-Bailey model. *Journal of Theoretical Biology* 188:109–120.
- Dwyer, G., J. Dushoff, J. Elkinton, J. P. Burand, and L. S. A. 2002. Variation in susceptibility: lessons from an insect virus. Pages 74–84 in K. S. U. Dieckmann and H. Metz, eds. *Adaptive dynamics of infectious diseases: in pursuit of virulence management*. Cambridge University Press, Cambridge.
- Dwyer, G., J. Dushoff, J. Elkinton, and S. Levin. 2000. Pathogen-driven outbreaks in forest defoliators revisited: building models from experimental data. *American Naturalist* 156:105–120.
- Dwyer, G., J. Dushoff, and S. H. Yee. 2004. The combined effects of pathogens and predators on insect outbreaks. *Nature* 430:341–345.
- Dwyer, G., and J. S. Elkinton. 1995. Host dispersal and the spatial spread of insect pathogens. *Ecology* 76:1262–1275.
- Dwyer, G., J. Elkinton, and J. Buonaccorsi. 1997. Host heterogeneity in susceptibility and disease dynamics: tests of a mathematical model. *American Naturalist* 150:685–707.
- Dwyer, G., J. Firestone, and T. Stevens. 2005. Should models of disease dynamics in herbivorous insects include the effects of variability in host-plant foliage quality? *American Naturalist* 165:16–31.
- Eakin, L., M. Wang, and G. Dwyer. 2015. The effects of the avoidance of infectious hosts on infection risk in an insect-pathogen interaction. *American Naturalist* 185:100–112.
- Elderd, B. D. 2013. Developing models of disease transmission: insights from ecological studies of insects and their baculoviruses. *PLoS Pathogens* 9:e1003372.
- Elderd, B. D., J. Dushoff, and G. Dwyer. 2008. Host-pathogen interactions, insect outbreaks, and natural selection for disease resistance. *American Naturalist* 172:829–842.
- Elderd, B. D., B. J. Rehill, K. J. Haynes, and G. Dwyer. 2013. Induced plant defenses, host-pathogen interactions, and forest insect outbreaks. *Proceedings of the National Academy of Sciences of the USA* 110:14978–14983.
- Elkinton, J. S., W. M. Healy, J. P. Buonaccorsi, G. H. Boettner, A. M. Hazzard, and H. R. Smith. 1996. Interactions among gypsy moths, white-footed mice, and acorns. *Ecology* 77:2332–2342.
- Elkinton, J. S., and A. M. Liebhold. 1990. Population dynamics of gypsy moth in North America. *Annual Review of Entomology* 35:571–596.

- Ellner, S. P. 2013. Rapid evolution: from genes to communities, and back again? *Functional Ecology* 27:1087–1099.
- Ellner, S. P., M. A. Geber, and N. G. Hairston. 2011. Does rapid evolution matter? measuring the rate of contemporary evolution and its impacts on ecological dynamics. *Ecology Letters* 14:603–614.
- Falconer, D., and T. Mackay. 1996. Introduction to quantitative genetics. Prentice Hall, Harlow.
- Fleming-Davies, A. E., V. Dukic, V. Andreasen, and G. Dwyer. 2015. Effects of host heterogeneity on pathogen diversity and evolution. *Ecology Letters* 18:1252–1261.
- Fleming-Davies, A. E., and G. Dwyer. 2015. Phenotypic variation in overwinter environmental transmission of a baculovirus and the cost of virulence. *American Naturalist* 186:797–806.
- Fuller, E., B. D. Elderd, and G. Dwyer. 2012. Pathogen persistence in the environment and insect-baculovirus interactions: disease-density thresholds, epidemic burnout, and insect outbreaks. *American Naturalist* 179:E70–E96.
- Funk, C. J., S. C. Braunagel, and G. F. Rohrmann. 1997. Baculovirus structure. Pages 7–32 in L. K. Miller, ed. *The baculoviruses*. Springer, Berlin.
- Fussmann, G. F., S. P. Ellner, K. W. Shertzer, and N. G. Hairston Jr. 2000. Crossing the hopf bifurcation in a live predator-prey system. *Science* 290:1358–1360.
- Godfray, H. C. J. 1994. Parasitoids: behavioral and evolutionary ecology. Princeton University Press, Princeton, NJ.
- Gould, J., J. Elkinton, and W. Wallner. 1990. Density-dependent suppression of experimentally created gypsy moth, *Lymantria dispar* (Lepidoptera: Lymantriidae), populations by natural enemies. *Journal of Animal Ecology* 59:213–233.
- Grove, M. J., and K. Hoover. 2007. Intrastadial developmental resistance of third instar gypsy moths (*Lymantria dispar* L.) to *L. dispar* nucleopolyhedrovirus. *Biological Control* 40:355–361.
- Hajek, A. E. 1999. Pathology and epizootiology of *Entomophaga mai-maiga* infections in forest Lepidoptera. *Microbiology and Molecular Biology Reviews* 63:814–835.
- Hajek, A. E., P. C. Tobin, and K. J. Haynes. 2015. Replacement of a dominant viral pathogen by a fungal pathogen does not alter the collapse of a regional forest insect outbreak. *Oecologia (Berlin)* 177:785–797.
- Haynes, K. J., A. M. Liebhold, T. M. Fearer, G. Wang, G. W. Norman, and D. M. Johnson. 2009a. Spatial synchrony propagates through a forest food web via consumer-resource interactions. *Ecology* 90: 2974–2983.
- Haynes, K. J., A. M. Liebhold, and D. M. Johnson. 2009b. Spatial analysis of harmonic oscillation of gypsy moth outbreak intensity. *Oecologia (Berlin)* 159:249–256.
- Henter, H., and S. Via. 1995. The potential for coevolution in a host-parasitoid system. 1. The potential genetic variation within an aphid population in susceptibility to a parasitic wasp. *Evolution* 49:427–438.
- Herzog, J., C. B. Mueller, and C. Vorburger. 2007. Strong parasitoid-mediated selection in experimental populations of aphids. *Biology Letters* 3:667–669.
- Hiltunen, T., N. G. Hairston Jr., G. Hooker, L. E. Jones, and S. P. Ellner. 2014. A newly discovered role of evolution in previously published consumer-resource dynamics. *Ecology Letters* 17:915–923.
- Hudson, A. I., A. E. Fleming-Davies, D. J. Páez, and G. Dwyer. 2016. Genotype-by-genotype interactions between an insect and its pathogen. *Journal of Evolutionary Biology* 29:2480–2490.
- Hunter, A. F., and J. S. Elkinton. 2000. Effects of synchrony with host plant on populations of a spring-feeding lepidopteran. *Ecology* 81: 1248–1261.
- Hunter-Fujita, F. R., P. F. Entwistle, and H. R. Evans. 1998. Insect viruses and pest management. Wiley, Chichester.
- Johnson, D. M., A. M. Liebhold, O. N. Bjørnstad, and M. L. McManus. 2005. Circumpolar variation in periodicity and synchrony among gypsy moth populations. *Journal of Animal Ecology* 74:882–892.
- Jones, C. G., R. S. Ostfeld, M. P. Richard, E. M. Schauber, and J. O. Wolff. 1998. Chain reactions linking acorns to gypsy moth outbreaks and Lyme disease risk. *Science* 279:1023–1026.
- Keeling, M. J., and P. Rohani. 2008. Modeling infectious diseases in humans and animals. Princeton University Press, Princeton, NJ.
- Kendall, B. E., C. J. Briggs, W. W. Murdoch, P. Turchin, S. P. Ellner, E. McCauley, R. M. Nisbet, and S. N. Wood. 1999. Why do populations cycle? a synthesis of statistical and mechanistic modeling approaches. *Ecology* 80:1789–1805.
- Kraaijeveld, A., J. Ferrari, and H. Godfray. 2002. Costs of resistance in insect-parasite and insect-parasitoid interactions. *Parasitology* 125: S71–S82.
- Liebhold, A., and N. Kamata. 2000. Are population cycles and spatial synchrony a universal characteristic of forest insect populations? *Population Ecology* 42:205–209.
- Liebhold, A. M., R. Plymale, J. S. Elkinton, and A. E. Hajek. 2013. Emergent fungal entomopathogen does not alter density dependence in a viral competitor. *Ecology* 94:1217–1222.
- McCullagh, P., and J. A. Nelder. 1989. Generalized linear models. Vol. 2. Chapman & Hall, London.
- McManus, M., and C. C. Doane. 1981. The gypsy moth: research toward integrated pest management. Technical bulletins 158053, USDA Economic Research Service.
- Menalled, F. D., R. K. D. Peterson, R. G. Smith, W. S. Curran, D. J. Páez, and B. D. Maxwell. 2016. The eco-evolutionary imperative: revisiting weed management in the midst of an herbicide resistance crisis. *Sustainability* 8:1297, doi:10.3390/su8121297.
- Moreau, G., and C. J. Lucarotti. 2007. A brief review of the past use of baculoviruses for the management of eruptive forest defoliators and recent developments on a sawfly virus in Canada. *Forestry Chronicle* 83:105–112.
- Murray, K. D., and J. S. Elkinton. 1989. Environmental contamination of egg masses as a major component of transgenerational transmission of gypsy-moth nuclear polyhedrosis virus (LdMNPV). *Journal of Invertebrate Pathology* 53:324–334.
- Myers, J. H. 1988. Can a general hypothesis explain population cycles of forest Lepidoptera? *Advances in Ecological Research* 18:179–242.
- . 1993. Population outbreaks in forest Lepidoptera. *American Scientist* 81:240–251.
- Narciso, D. 2014. Some central Ohioans object to gypsy-moth spraying. *Columbus Dispatch* (February 17).
- Nealis, V. G. 1991. Parasitism in sustained and collapsing populations of the jack pine budworm, *Choristoneura pinus* Free. (Lepidoptera: Tortricidae), in Ontario, 1985–1987. *Canadian Entomologist* 123:1065–1075.
- Nolan, I. 2015. State agency plans second meeting to update gypsy moth plan. Island Free Press (October 27).
- Páez, D. J., V. Dukic, J. Dushoff, A. Fleming-Davies, and G. Dwyer. 2017. Data from: Eco-evolutionary theory and insect outbreaks. *American Naturalist*, Dryad Digital Repository, <http://dx.doi.org/10.5061/dryad.8mv03>.
- Páez, D. J., A. E. Fleming-Davies, and G. Dwyer. 2015. Effects of pathogen exposure on life history variation in the gypsy moth (*Lymantria dispar*). *Journal of Evolutionary Biology* 28:1828–1839.

- Parker, B. J., S. M. Baribeau, A. M. Laughton, J. C. de Roode, and N. M. Gerardo. 2011. Non-immunological defense in an evolutionary framework. *Trends in Ecology and Evolution* 26:242–248.
- Plummer, M., N. Best, K. Cowles, and K. Vines. 2006. CODA: convergence diagnosis and output analysis for MCMC. *R News* 6:7–11.
- Podgwaite, J. D., N. R. Dubois, R. C. Reardon, and J. Witcosky. 1993. Retarding outbreak of low-density gypsy-moth (*Lepidoptera: Lymantriidae*) populations with aerial applications of gypchek and *Bacillus thuringiensis*. *Journal of Economic Entomology* 86:730–734.
- Podgwaite, J. D., R. C. Reardon, G. S. Walton, and J. Witcosky. 1992. Efficacy of aerially-applied Gypchek against gypsy-moth (*Lepidoptera: Lymantriidae*) in the Appalachian Highlands. *Journal of Entomological Sciences* 27:337–344.
- Reilly, J. R., and B. D. Elderd. 2014. Effects of biological control on long-term population dynamics: identifying unexpected outcomes. *Journal of Applied Ecology* 51:90–101.
- Rozins, C., and T. Day. 2016. The industrialization of farming may be driving virulence evolution. *Evolutionary Applications* 10:189–198.
- Sasaki, A., and H. C. J. Godfray. 1999. A model for the coevolution of resistance and virulence in coupled host-parasitoid interactions. *Proceedings of the Royal Society B* 266:455–463.
- Schreiber, S. J., R. Bürger, and D. I. Bolnick. 2011. The community effects of phenotypic and genetic variation within a predator population. *Ecology* 92:1582–1593.
- Skaller, P. M. 1985. Patterns in the distribution of gypsy moth (*Lymantria dispar*) egg masses over an 11 year population cycle. *Environmental Entomology* 14:106–117.
- Turchin, P. 2003. Complex population dynamics: a theoretical/empirical synthesis. *Monographs in Population Biology*. Princeton University Press, Princeton, NJ.
- Walter, J. A., D. M. Johnson, P. C. Tobin, and K. J. Haynes. 2015. Population cycles produce periodic range boundary pulses. *Ecography* 38:1200–1211.
- Watanabe, H. 1987. The host population. Pages 71–112 in J. Fuxa and Y. Tanada, eds. *Epizootiology of insect diseases*. Wiley, New York.
- Williams, D. W., R. W. Fuester, W. W. Metterhouse, R. J. Balaam, R. H. Bullock, R. J. Chianese, and R. C. Reardon. 1990. Density, size and mortality of egg masses in New Jersey populations of the gypsy moth (*Lepidoptera, Lymantriidae*). *Environmental Entomology* 19: 943–948.
- Woods, S. A., and J. S. Elkinton. 1987. Bimodal patterns of mortality from nuclear polyhedrosis-virus in gypsy-moth (*Lymantria dispar*) populations. *Journal of Invertebrate Pathology* 50:151–157.
- Yoshida, T., S. P. Ellner, L. E. Jones, B. J. M. Bohannan, R. E. Lenski, and N. G. Hairston Jr. 2007. Cryptic population dynamics: rapid evolution masks trophic interactions. *PLoS Biology* 5:1868–1879.
- Yoshida, T., L. E. Jones, S. P. Ellner, G. F. Fussmann, and N. G. Hairston. 2003. Rapid evolution drives ecological dynamics in a predator-prey system. *Nature* 424:303–306.
- Zbinden, M., C. R. Haag, and D. Ebert. 2008. Experimental evolution of field populations of *Daphnia magna* in response to parasite treatment. *Journal of Evolutionary Biology* 21:1068–1078.

Associate Editor: Mathew A. Leibold
Editor: Alice A. Winn

Appendix B from D. J. Páez et al., “Eco-Evolutionary Theory and Insect Outbreaks” (Am. Nat., vol. 189, no. 6, p. 000)

Alternative Models

As we mention in the main text, we considered alternative models as a way of testing the generality of our results. In the first of these alternatives, we eliminated stochasticity and the generalist predator, and we assumed that the epizootic model (eqq. [1]–[4]) always proceeds to burnout (Keeling and Rohani 2008), meaning that the epidemic ends because of a lack of susceptible hosts rather than because of pupation (Dwyer et al. 2000). Strictly speaking, the burnout approximation requires the assumption that $t \rightarrow \infty$, but the burnout approximation’s prediction of the cumulative fraction infected is nevertheless often close to the prediction of equations (1)–(4) when the epizootic length is a realistic 8 weeks (Fuller et al. 2012). Allowing epizootics to end because of pupation instead of burnout is quantitatively important when we attempt to reproduce outbreak cycles, because when epizootics are only 8 weeks long, the model produces longer-period, larger-amplitude cycles that better match the outbreak data (Fuller et al. 2012), but including a model that allows for burnout allows us to use qualitative stability analysis, which permits a deeper understanding of the effects of natural selection on population cycles.

Given these simplifications, and in the absence of generalist predation, equations (5)–(7) become

$$N_{n+1} = N_n[1 - i(N_n, Z_n, \bar{v}_n)]\{r + rs\bar{v}_n[1 - i(N_n, Z_n, \bar{v}_n)]^V\}, \quad (\text{B1})$$

$$Z_{n+1} = fN_n i(N_n, Z_n, \bar{v}_n) + \gamma Z_n, \quad (\text{B2})$$

$$\bar{v}_{n+1} = v_n[1 - i(N_n, Z_n, \bar{v}_n)]^{bV} \frac{\{1 + s\bar{v}_n(bV + 1)[1 - i(N_n, Z_n, \bar{v}_n)]^{bV}\}}{1 + s\bar{v}_n[1 - i(N_n, Z_n, \bar{v}_n)]^{bV}}. \quad (\text{B3})$$

Here the fraction of infected individuals, i , is represented by the burnout approximation, which is calculated from equations (1)–(4) by allowing $t \rightarrow \infty$. In that case, we can write down an implicit expression for i :

$$1 - i(N_n, Z_n, \bar{v}_n) = \{1 + \bar{v}_n V[N_n i(N_n, Z_n, \bar{v}_n) + Z_n]\}^{-1/V}. \quad (\text{B4})$$

Using this expression in equations (B1)–(B3) produces a model for which we can carry out stability analysis.

The initial step is to calculate the model equilibria. For this model, we cannot prove that there is only one nonzero equilibrium, but two lines of indirect evidence suggest that multiple equilibria are unlikely unless baseline fecundity $r > 1$. First, if we set $b = 1$, equations (1)–(4) are the same as the no-predator model from Elderd et al. (2008), for which it is possible to prove that $r < 1$ guarantees that there is only one equilibrium. We have not been able to prove a similar result for equations (B1)–(B4), but numerical iteration of the model suggests that multiple equilibria are at least unlikely unless r is quite close to 1, as we will show. These considerations are important because a lack of multiple equilibria makes numerical calculation of the Jacobian matrix reasonably straightforward. To write down the Jacobian, we first rescale the model by defining

$$\hat{N}_n \equiv \mu s N_n, \quad (\text{B5})$$

$$\hat{Z}_n \equiv \frac{\mu s}{\eta} Z_n, \quad (\text{B6})$$

$$\hat{\bar{v}}_n \equiv \frac{1}{s} \bar{v}_n. \quad (\text{B7})$$

For convenience, we also define $h \equiv 1 - i(N_n, Z_n, \bar{v}_n)$, where the fraction infected $i(N_n, Z_n, \bar{v}_n)$ is calculated from equation (B4). This gives

$$\hat{N}_{n+1} = \hat{N}_n h[r + r\hat{\bar{\nu}}_n h^V], \quad (\text{B8})$$

$$\hat{Z}_{n+1} = \phi\hat{N}_n(1 - h) + \gamma\hat{Z}_n, \quad (\text{B9})$$

$$\hat{\bar{\nu}}_{n+1} = \frac{\hat{\bar{\nu}}_n h^{bV} + (bV + 1)\hat{\bar{\nu}}_n^2 h^{2bV}}{1 + \hat{\bar{\nu}}_n h^{bV}}, \quad (\text{B10})$$

$$h = [1 + \hat{\bar{\nu}}_n V(\hat{N}_n h + \hat{Z}_n)]^{-1/V}. \quad (\text{B11})$$

We can then use equations (B8)–(B11) to find the equilibrium, such that $\hat{N}_{n+1} = \hat{N}_n$, $\hat{Z}_{n+1} = \hat{Z}_n$, and $\hat{\bar{\nu}}_{n+1} = \hat{\bar{\nu}}_n$. Also, for convenience, we drop the hat symbols and use asterisks to label the equilibrium values of the state variables:

$$N^* = \frac{\hat{h}^{-V}(\hat{h}^V - 1)(\gamma - 1)}{\bar{\nu}V(1 - \hat{h})(\gamma - \phi - 1)}, \quad (\text{B12})$$

$$Z^* = \frac{\phi N(\hat{h} - 1)}{\gamma - 1}, \quad (\text{B13})$$

$$\bar{\nu}^* = \frac{1 - \hat{h}r}{r\hat{h}^{V+1}}. \quad (\text{B14})$$

Here \hat{h} is the fraction of individuals uninfected at equilibrium. By replacing $\bar{\nu}$ in equation (B10) with the right-hand side of equation (B14), we can write an implicit expression for \hat{h} , which we can easily solve numerically:

$$(bV + 1)(\hat{h}r - 1)\hat{h}^{2bV} - r\hat{h}^{(b+1)V+1} = (\hat{h}r - 1)\hat{h}^{bV} - r\hat{h}^{V+1}. \quad (\text{B15})$$

Plotting the left- and right-hand sides of this equation for a range of parameter values suggests that for $r < 1$, there is only one internal equilibrium, but for $r > 1$, two equilibria often occur, with dynamics that generally lead to the extinction of the pathogen population. Given that realistic values of r are below 1, in what follows we concentrate on the case for which $r < 1$.

Next, we define $F(N_n, Z_n, \bar{\nu}_n) \equiv N_{n+1}$, $G(N_n, Z_n, \bar{\nu}_n) \equiv Z_{n+1}$, and $H(N_n, Z_n, \bar{\nu}_n) \equiv \bar{\nu}_{n+1}$, and we differentiate each function with respect to N_n , Z_n , and $\bar{\nu}_n$ to produce the Jacobian matrix. To do this, we first differentiate h with respect to N , Z , and $\bar{\nu}$:

$$\frac{\partial h}{\partial N} = \frac{(1 - h)\bar{\nu}}{\bar{\nu}N - \{1 - \bar{\nu}V[N(1 - h) + Z]\}^{1/V+1}}, \quad (\text{B16})$$

$$\frac{\partial h}{\partial Z} = \frac{\bar{\nu}}{\bar{\nu}N - \{1 + \bar{\nu}V[N(1 - h) + Z]\}^{1/V+1}}, \quad (\text{B17})$$

$$\frac{\partial h}{\partial \bar{\nu}} = \frac{(1 - h)N + Z}{\bar{\nu}N - \{1 + \bar{\nu}V[N(1 - h) + Z]\}^{1/V+1}}. \quad (\text{B18})$$

The matrix of partial derivatives is then described by the matrix \mathbf{J} :

$$\mathbf{J} = \begin{bmatrix} 1 + Nr \frac{\partial h}{\partial N} [\bar{v}(V+1)h^V + 1] & Nr \frac{\partial h}{\partial Z} [\bar{v}(V+1)h^V + 1] & Nr \left\{ h^V \left[\bar{v}(V+1) \frac{\partial h}{\partial \bar{v}} + h \right] + \frac{\partial h}{\partial \bar{v}} \right\} \\ \phi \left[(1-h) - \frac{\partial h}{\partial N} \right] & \gamma - \phi N \frac{\partial h}{\partial Z} & - \frac{\partial h}{\partial \bar{v}} \phi N \\ \frac{b\bar{v}V \frac{\partial h}{\partial N} [\bar{v}(bV+1)(\bar{v}h^{bV} + 2)h^{bV-1} + 1]h^{bV-1}}{(\bar{v}h^{bV} + 1)^2} & \frac{b\bar{v}V \frac{\partial h}{\partial Z} [\bar{v}(bV+1)(\bar{v}h^{bV} + 2)h^{bV-1} + 1]h^{bV-1}}{(\bar{v}h^{bV} + 1)^2} & \frac{h^{bV-1} [vh^{bV}(bV+1)(vh^{bV} + 2) + 1] \left(bV \frac{\partial h}{\partial v} + h \right)}{(vh^{bV} + 1)^2} \end{bmatrix}$$

By numerically solving equation (B15) for the equilibrium value \hat{h} , we can calculate the equilibrium values of the state variables N^* , Z^* , and \bar{v}^* , and insert them into the matrix \mathbf{J} to construct the Jacobian matrix. We can then numerically solve for values of the parameters for which the Jacobian has one real eigenvalue and a complex pair of eigenvalues with modulus 1, the criterion that defines the boundary between a stable point equilibrium and a Hopf bifurcation and thus population cycles. In figure 1, the shading denotes periods and amplitudes as calculated by numerical iteration of equations (B8)–(B11), while the unshaded region is the area within which only a stable point equilibrium occurred. The dashed line in figure 1 then shows that the eigenvalue prediction of the boundary between cycles and a stable equilibrium point generally matches the boundary between cycles and a stable equilibrium from the numerical iterations, confirming both calculations. At higher heritability, however, the stability calculation breaks down for very high values of the fecundity cost r . In that region, it appears that the model may show multiple equilibria, with the proviso that such high values of r are unlikely to be biologically realistic and are therefore of limited interest.

 More generally, figure 1 shows that in contrast to equations (5)–(7), for this model, low values of heritability are generally stabilizing. As we described in the main text, this difference is most likely due to the assumption here that epizootics are terminated by burnout rather than by pupation. Pupation tends to terminate epizootics sooner than burnout, exacerbating the effects of the delayed density dependence that drives cycles (Fuller et al. 2012) and leading to greater instability at low heritability. This eliminates the long periods and large amplitudes seen at low heritability in figure 3 as well as the area of dramatic oscillations at high heritability and intermediate costs in that figure. On the other hand, when the baseline fecundity r is high in figure 1, a stable, point equilibrium is most likely at intermediate heritability, so that low heritability can be destabilizing when costs are high.

We also considered a host-parasitoid model, in which there is only one parasitoid generation per host generation, as compared with the multiple pathogen generations per host generation in equations (1)–(4). As in equations (1)–(4), however, we again allow for host variation, this time at the risk of being successfully attacked by the parasitoid. We then have a closed-form expression for the fraction infected (Godfray 1994):

$$i = 1 - (1 + \bar{v}_n V Z_n)^{-1/V}. \quad (\text{B19})$$

We then again add a generalist predator on the grounds that high levels of generalist predator attacks have been observed not just in defoliators  whose outbreaks are driven by pathogens, but also in defoliators, in which outbreaks are instead driven by parasitoids  (Wyller et al. 2004). The model then differs from the multigeneration model (eqq. [5]–[7]) only in using equation (B19) to calculate the fraction infected $i(N_n, Z_n, \bar{v}_n)$.

Figure B2 shows a time series of the host-parasitoid model dynamics to show that consumer-resource cycles are again partly driven by fluctuations in the average risk of attack, as in equations (5)–(7). Also, figure B3 shows the average period and the average amplitude for this model for a range of parameters, as in figure 3. The effects of the parameters on the host-parasitoid-predator model are thus qualitatively similar to the effects of the parameters on the host-pathogen-predator model, with the proviso that for values of heritability much above 0.4, the parasitoid becomes extinct unless the cost parameter r is close to 1. This instability likely occurs because the parasitoid has only one generation per year, which exacerbates the effects of the delayed density dependence that drives cycles, and because of the lack of a parasitoid functional response, which we have omitted to allow for a more straightforward comparison to the model in the main text. Also, low heritability is again at least weakly destabilizing, as in the model in the main text, most likely because the host-parasitoid model includes the same severe delayed density dependence as the model in the main text.

Details of Insect Rearing Methods

Wild egg masses were collected from five different sites in the Midwestern United States (Páez et al. 2015). Previous work has shown that geographic structure in infection risk across gypsy moth populations is slight (Elder et al. 2008), and

previous dose-response experiments showed that these particular populations had very similar responses in laboratory dose-response experiments (Fleming-Davies et al. 2015). It therefore appeared that infection risk in the field would not differ systematically between populations.

Before hatch, we soaked all egg masses in a 4% formalin solution, which surface sterilizes the eggs by killing any occlusion bodies on their surface. This kept virus mortality in control treatments low, as it has been in previous experiments (Elder et al. 2008; Fuller et al. 2012). Hatching larvae were then reared in groups of 30 in 177-mL (6 oz) plastic cups containing 50–100 mL of artificial diet at 25°C in an incubator with a 14L:10D cycle, following long-established rearing procedures for this insect (McManus and Doane 1981).

To produce larvae of different relatedness for experiments, we reared insects from wild-collected egg masses to adulthood, and we mated the adults usually within 24 h of female emergence. Full siblings can be easily produced by exposing one male to one female, but to produce half siblings, we instead exposed one male to two to three virgin females every 24 h (Páez et al. 2015). After reproduction and egg mass deposition, we allowed 28 days of prediapause at 25°C, and then we induced diapause by cooling the egg masses to 5°C for 9–10 months.

The most important rounds of transmission in nature occur when larvae are in the fourth instar (Woods and Elkinton 1987), and so we used fourth instars in all of our experiments. Infection risk given virus exposure can vary even within an instar (Grove and Hoover 2007), however, so we also synchronized the development of the uninfected insects before deployment in the field. To do this, we collected larvae in the third instar whose head capsules had slipped forward, indicating that they were within 24 h of molting to the next instar. We then held these insects at 5°C in the lab until we had enough fourth instars to begin an experiment, which typically took 48 h. Using developmentally synchronized larvae helps to eliminate extrabinomial variance (Elder et al. 2008).

Calculating Fecundity Costs including Lab-Reared Insects and Allowing for Density-Independent Mortality

As we mentioned in the main text, in estimating the cost of resistance, we included only insects that had survived virus exposure in the field, but in a second analysis, we included insects reared in the lab, where larvae could not encounter the virus. Here we present the results from this second analysis. As in the first analysis, we used a linear mixed effects model in which pupal weight was a function of infection risk ν and random family effects, but we also included the effects of the rearing method, meaning lab versus field. Again as we mentioned in the main text, Akaike information criterion analysis of these models showed that the best model for the combined data included different intercepts, reflecting the higher pupal weights associated with consumption of artificial diet, but there was nevertheless a common slope for field-reared and lab-reared insects (table B1; fig. B4). The fecundity cost of reduced infection risk was thus indistinguishable for field-reared and lab-reared insects.

q6 

Table B1: Akaike information criterion (AIC) analysis for models fit to data for both lab-reared and field-reared insects

No.	Model	ΔAIC	AIC weight
1	Intercepts differ, slopes same	0	.88
2	Intercepts differ, slopes differ	1.97	.12
3	Intercepts differ, slopes = 0	12.6	<10 ⁻⁵
4	Intercepts and slopes same	54.6	<10 ⁻⁵
5	Intercepts same, slopes = 0	63.2	<10 ⁻⁵

Note: “Intercepts differ” means that the intercepts were different for the two groups and likewise for the slopes.

To estimate the uncertainty in the parameters of the regression lines, we bootstrapped the best model 10,000 times, such that at each iteration, the model was refit using resampled values of pupal weights and infection risks ν . These results showed that the median intercept for field-reared insects was 0.73 (upper and lower 95th percentiles = 0.70, 0.80), the median (common) slope was 0.45 (upper and lower 95th percentiles = 0.09, 0.56), and the median intercept for laboratory-reared insects was 0.97 (upper and lower 95th percentiles = 0.93, 1.05). The lower confidence bound on the slope parameter does not include 0, and we therefore conclude that including lab-reared insects does not affect our conclusion that there is a significant relationship between infection risk ν and pupal weight.

As we described in the main text, to estimate the cost parameters r and s , we converted from pupal weight to egg number using previously published conversion factors (Dwyer and Elkinton 1995; Páez et al. 2015), and we also allowed for mortality of early instars using previously published mortality estimates (Hunter and Elkinton 2000). We then accounted for the uncertainty in the conversions by bootstrapping the relevant data, and we used the resulting resampled model coefficients to calculate r and s . Our estimates for field-reared F and lab-reared L insects were then $S_F = 1.21$ (0.2, 1.9), $r_F = 0.22$ (0.05, 0.51) and $s_L = 0.74$ (0.13, 1.03), $r_L = 0.36$ (0.08, 0.76).

Details of Statistical Analyses

In our likelihood function for our heritability models, we described the chance of infection using a binomial distribution (McCullagh and Nelder 1989). Meanwhile, standard quantitative genetic practice is to assume that the effects due to sire, dam, and experimental day follow normal distributions with mean 0 (Falconer and Mackay 1996). Our likelihood function is therefore

$$\ell(\nu^*, V, S_j, M_k, D_l, \sigma_S^2, \sigma_M^2, \sigma_D^2 | y_{jkl}, n_{jkl}) = \left\{ \sum_{j=1}^{37} \sum_{k=1}^{83} \sum_{l=1}^6 y_{jkl} \log[p_{jkl}(\nu^*, V, S_j, M_k, D_l)] + (n_{jkl} - y_{jkl}) \log[1 - p_{jkl}(\nu^*, V, S_j, M_k, D_l)] \right\} + \sum_{j=1}^{37} \log \left\{ \frac{1}{\sqrt{2\pi\sigma_S^2}} e^{-[(S_j)^2/2\sigma_S^2]} \right\} + \sum_{k=1}^{83} \log \left\{ \frac{1}{\sqrt{2\pi\sigma_M^2}} e^{-[(M_k)^2/2\sigma_M^2]} \right\} + \sum_{l=1}^6 \log \left\{ \frac{1}{\sqrt{2\pi\sigma_D^2}} e^{-[(D_l)^2/2\sigma_D^2]} \right\}. \quad (\text{B20})$$

Here $\ell(\nu^*, V, S_j, M_k, D_l, \sigma_S^2, \sigma_M^2, \sigma_D^2 | y, n)$ is the log-likelihood of the transmission parameters ν^* and V , the sire effect S_j , the maternal effect M_k , the day effect D_l , and the corresponding variances σ_S^2 , σ_M^2 , and σ_D^2 , given the number infected y_{jkl} and the number initially infected n_{jkl} . Also, $p_{jkl}(\nu^*, V, S_j, M_k, D_l)$ is the prediction of the transmission equation (10), again given baseline infection risk ν^* , squared coefficient of variation V , sire effect S_j , dam effect M_k , and start-day effect D_l . The bounds on the summations reflect the number of treatments, such that there were 37 sires, 83 dams, and six start days. Estimating heritability therefore required that we estimate σ_S^2 , σ_M^2 , and σ_D^2 , which in turn required that we simultaneously estimate the random effect sizes S_j , M_k , and D_l as well as the baseline infection risk ν^* and the squared coefficient of variation V .

To do this, we used a Bayesian hierarchical model, in combination with a Metropolis-Hastings Markov chain Monte Carlo (MCMC) algorithm. Specifically, we used 10 MCMC chains that were sampled every one thousandth step over 1.5×10^6 steps after discarding the first 1.5×10^4 steps. Chain convergence was confirmed using the Gelman-Rubin diagnostic criterion (Plummer et al. 2006). To calculate heritability, we then inserted the sets of values of σ_S^2 , σ_M^2 , and σ_D^2 from the posterior distribution of the parameters into the heritability equation (9). This produced a distribution of heritability values b , from which we calculated the median and 95% highest posterior density (HPD) interval.

As we mentioned in the main text, visual inspection of plots of model predictions and observed infection rates versus virus densities did not provide a useful diagnostic of goodness of fit. As an alternative diagnostic, we therefore instead plot observed infection rates versus the predictions for the best model (fig. B5). In principle, if the model explained all the variability in the data, each point would fall on the 1:1 line, but in practice, we of course expect significant variation around this line (Bolker 2008). As the figure shows, however, the points for the model nevertheless cluster around the 1:1 line, suggesting that the model is reasonably accurate.

Effects on the Model Predictions of Variation in Cost-Scaling s and Long-Term Pathogen Survival γ

Figure B6 shows that increasing the value of s to 1.9 (the upper bound on its 95% HPD) leads to periods and amplitudes that are almost identical to the periods and amplitudes seen when the cost-scaling parameter $s = 1.21$, the median value of s , as shown by comparison to figure 3. The major difference between the two cases is that when $s = 1.9$, the large-amplitude, long-period fluctuations that occur at high heritability for $s = 1.21$ are almost eliminated. Meanwhile,

figure B7 shows that reducing s to 0.2 (the lower bound on the 95% HPD) gives periods and amplitudes that are only modestly larger, at least for realistic values of heritability b and baseline fecundity r . When heritability is higher, however, the wild fluctuations that occur at intermediate fecundity cost r are so dramatic that the host and/or pathogen often becomes extinct (white space in fig. B7). Reductions in the cost parameter s are thus mildly destabilizing, unless heritability is very high.

Other than at high heritability, reductions in the cost parameters s and r are thus generally destabilizing. This is because at low virus densities, low values of r and s reduce the intensity of selection for increased fecundity. It then takes longer for the host population to recover to outbreak levels, leading in turn to more dramatic fluctuations in host and pathogen densities.

Reductions in the long-term pathogen survival parameter γ also have complex effects. As figure B8 shows, simply reducing γ leads to shorter periods and smaller amplitudes, although both periods and amplitudes again fall in a roughly realistic range. This effect likely occurs because lower pathogen survival leads to reduced selection intensity and thus less violent fluctuations in population densities. Reduced long-term survival, however, also increases the chance that the pathogen will become extinct, increasing the size of the region at high heritability for which the host and/or the pathogen becomes extinct.

Figure B9 again shows periods and amplitudes when $\gamma = 0.1$, but for values of the cost-scaling parameter $s = 0.2$, the lower bound on the 95% HPD. Here γ has similar effects to when $s = 1.21$, except that periods are longer and amplitudes are larger, and the region of pathogen extinction is also larger. Given that reductions in cost-scaling s have similar effects to reductions in baseline fecundity r , both effects are what we would expect for reduced values of s .

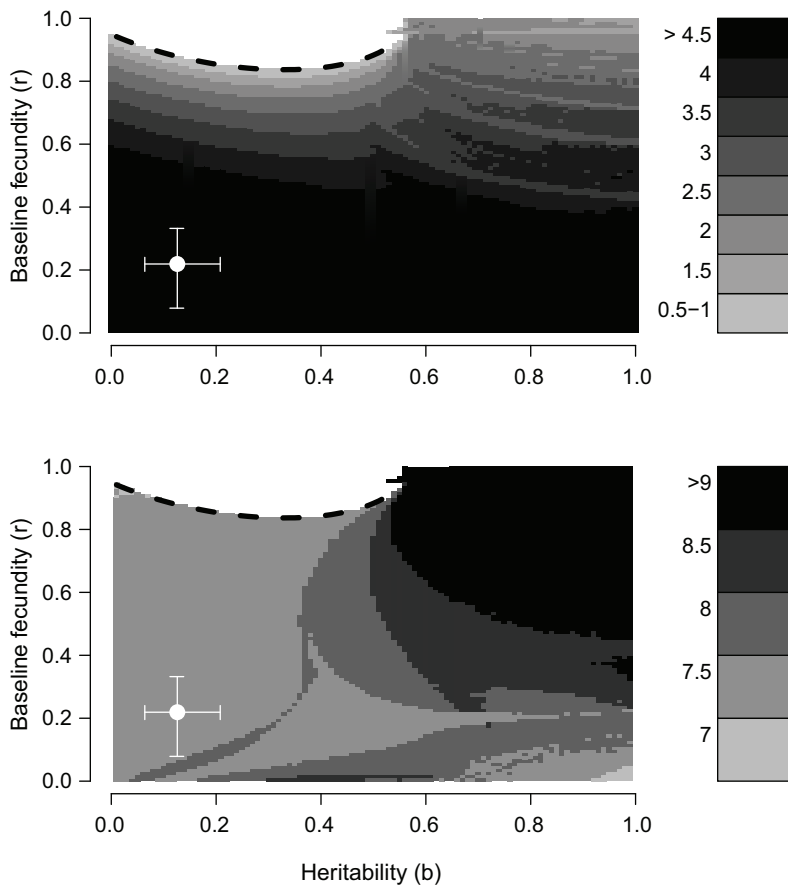


Figure B1: Average amplitude (top) and period (bottom) of population cycles in equations (B1)–(B4) for different combinations of the heritability of infection risk b and baseline reproduction r . White space at high baseline fecundity and low to moderate heritability indicates regions in which a stable equilibrium point occurs.

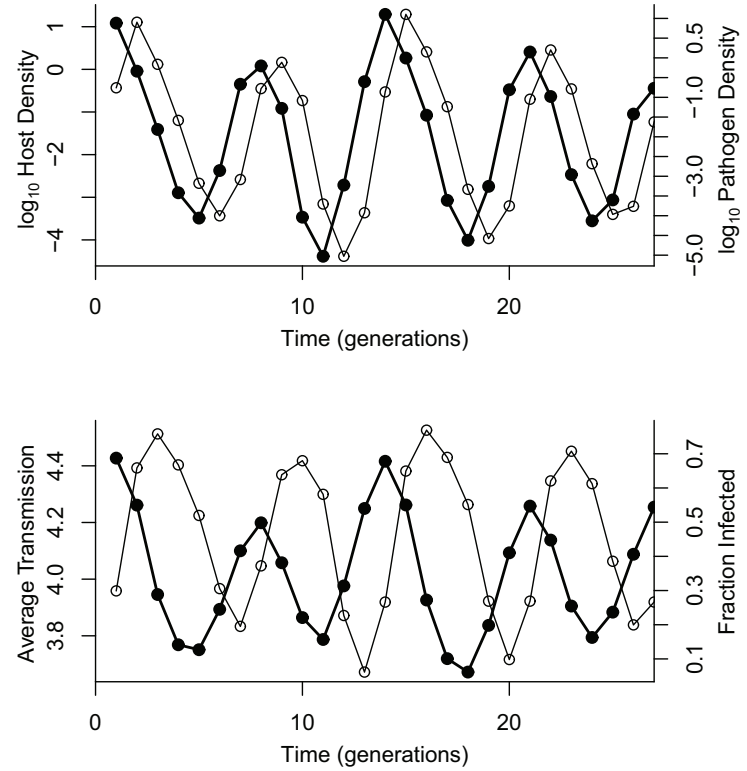


Figure B2: Predictions of an eco-evolutionary host-parasitoid model. As in figure 1, top panel shows changes in host and parasitoid density (black and gray lines, respectively), while bottom panel shows the corresponding changes in the parasitoid attack rate and the fraction infected (black and gray lines, respectively). Parameter values are $b = 0.13$, $r = 0.42$, $s = 0.5$, $V = 10$, $\gamma = 0.3$, $\phi = 1.0$, $a = 0.96$, $w = 0.14$.

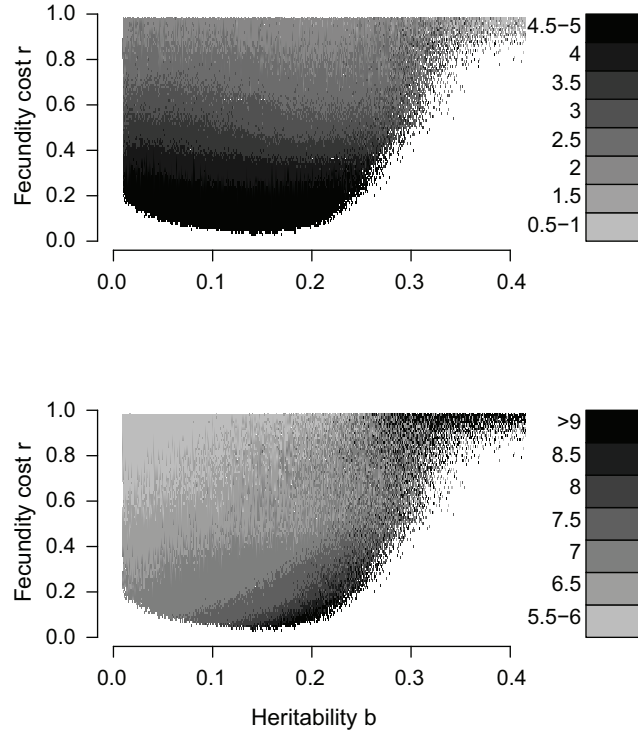


Figure B3: Effects of baseline fecundity r and heritability b on the period and amplitude of outbreak cycles in the eco-evolutionary host-parasitoid model. Top panel shows average cycle amplitudes in orders of magnitude, while bottom panel shows the average period in years.

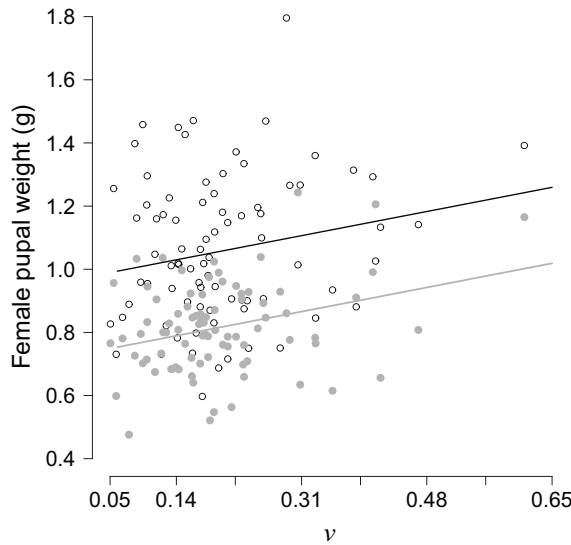


Figure B4: Relationship between infection risk ν and female pupal weight, including both insects that survived the field experiment (filled circles and gray line) and unexposed insects that were reared only in the lab (open circles and black line). Lines are based on median values for the average model coefficients from a bootstrapping procedure. The lower average weights of survivors of the experiment likely occurred because those larvae fed for a week on foliage rather than solely on artificial diet (Páez et al. 2015).

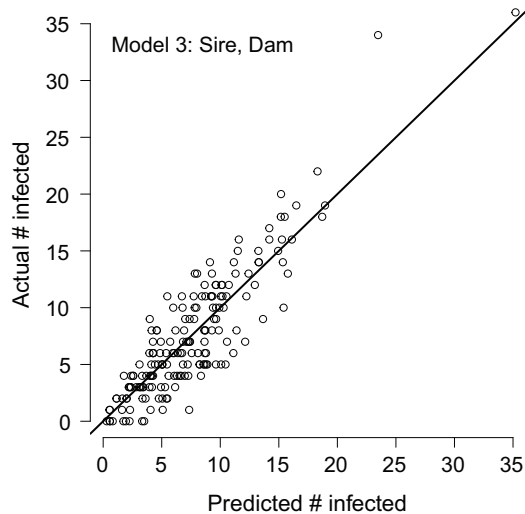


Figure B5: Predicted versus observed infection rates for the best-fit model of the heritability experiment. Also included is a 1:1 line to show the extent to which the model predictions deviate from a hypothetical perfect fit.

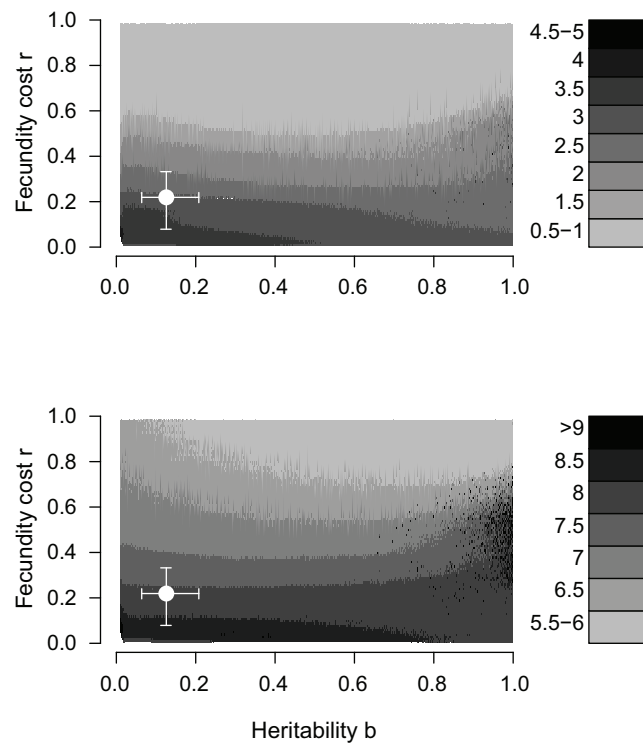


Figure B6: Effects of baseline fecundity r and heritability b on the period and amplitude of outbreak cycles in the long-term model (eqq. [5]–[7]), as in figure 3, except that here the cost-scaling parameter $s = 1.9$. Top panel shows average cycle amplitudes in orders of magnitude, while bottom panel shows the average period in years.

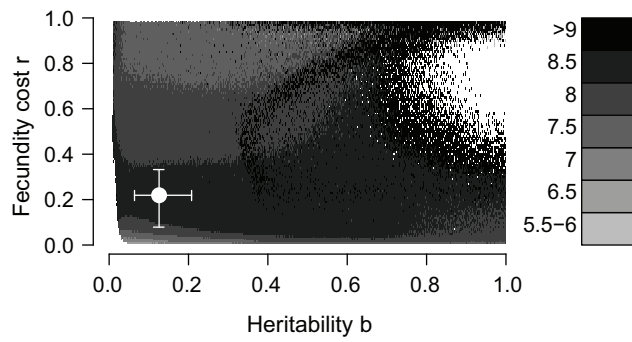
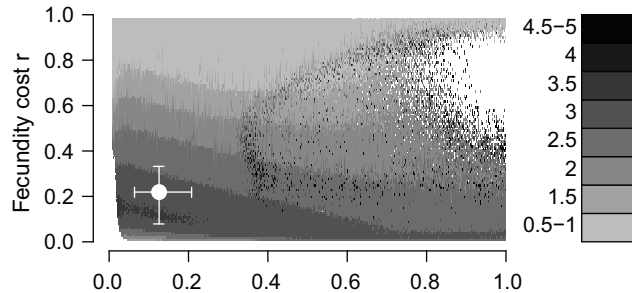


Figure B7: As in figure 3, except that the cost-scaling parameter $s = 0.2$. White areas show parameter values for which the host or the pathogen population became extinct for all 25 realizations at a given parameter combination.

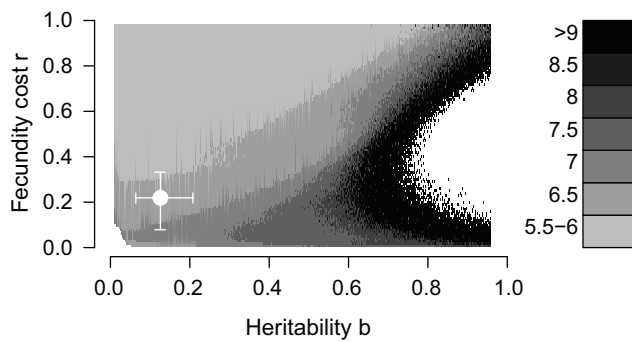
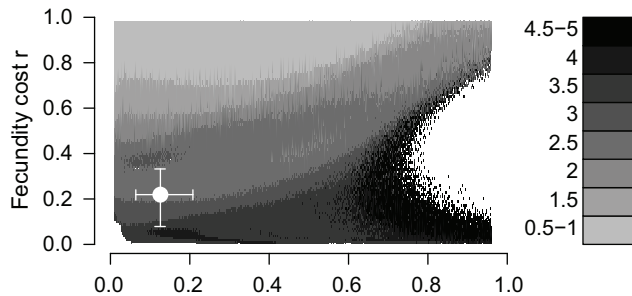


Figure B8: As in figure B7, except that the long-term pathogen survival parameter $\gamma = 0.1$.

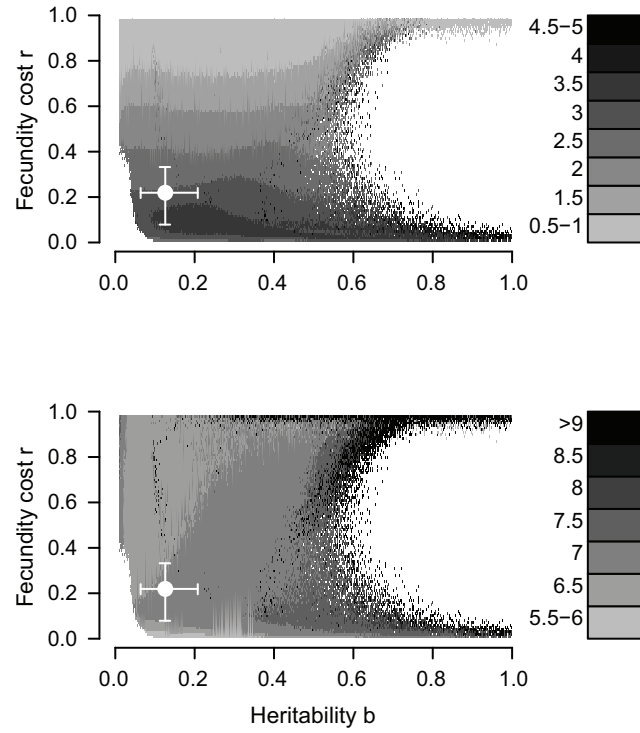


Figure B9: As in figure B7, except that the cost-scaling parameter $s = 0.2$, and the long-term pathogen survival parameter $\gamma = 0.1$.

QUERIES TO THE AUTHOR

Q1. AU: Your article has been edited by University of Chicago Press manuscript editors for grammar, clarity, consistency, and conformity to AN style. Please read the proof of your article carefully to make sure that your meaning has been retained. Note that we may be unable to make revisions that conflict with journal style or create grammatical problems. This proof is your final check of the text; once it has been placed on the web as an ahead-of-print article, it is considered published. Thank you.

Q2. AU: Please indicate Haynes et al. 2009a or 2009b.

Q3. AU: In figure 3, is there a word missing in “an average over 25”?

Q4. AU: Please indicate Haynes et al. 2009a or 2009b.

Q5. AU: Please indicate Haynes et al. 2009a or 2009b.

Q6. AU: In table B1, please define boldface values.

The American Naturalist
The University of Chicago Press
1427 East 60th Street
Chicago, Illinois 60637

FAX THIS FORM TO 773-753-3616
(fax provides the most security)

Information for Invoicing

Please fill out the information below to help the Journals Billing Office generate the invoice and direct it to the appropriate people. **If this form is not filled out, the invoice will go to the corresponding author.** The invoice will be generated after the issue is paginated. If you need an invoice sooner than that, please contact the journal office. **An author with an outstanding debt from a previous paper cannot publish another until the original debt is settled.**

IF YOU ARE PAYING WITH CHECKS OR PURCHASE ORDERS:

- Purchase orders will not be processed without a number.
- Please list vendor as *The University of Chicago Press, 11030 Langley Avenue, Chicago, Illinois 60623*
- If the purchase order is sent separately from this form, it must be marked **"confirming"** and mailed to *Cindy Garrett, Journals Division, The University of Chicago Press, 1427 East 60th Street, Chicago, Illinois 60637*.
- All purchase orders must include the following information:
 - Name of journal, Issue date (month and year—see proofs), Author's name, Amount of the invoice
- Make checks and purchase orders payable to ***The University of Chicago Press***

ELECTRONIC TRANSFER INFORMATION:

- Financial Institution: The Northern Trust Bank, 50 S. LaSalle Street, Chicago IL 60675; Account number: 2725681, Routing number: 071000152, Account name: University of Chicago Press, SWIFT: CNORUS44

Article Information

Volume _____ Issue _____ Month _____ Year _____
Manuscript No. _____

Author(s) _____

Title _____

Open Access: Yes No

Payment Method

1. Institutional Purchase Order No. _____
Purchase Order: attached to come
2. Check or Money Order No. _____
3. Electronic Fund Transfer
4. Credit Card: Visa MasterCard American Express Discover
Name as it appears on card: _____
Card number: _____
Exp. Date: _____ 3-4 Digit Security Code: _____
Signature: _____
Phone number: _____ E-mail: _____

Address of the Person Who Should Receive the Invoice

Mail (REQUIRED): _____

E-mail (REQUIRED): _____

The American Naturalist
The University of Chicago Press
1427 East 60th Street
Chicago, Illinois 60637

FAX THIS FORM TO 773-753-3616
(fax provides the most security)

Information for Invoicing

Please fill out the information below to help the Journals Billing Office generate the invoice and direct it to the appropriate people. **If this form is not filled out, the invoice will go to the corresponding author.** The invoice will be generated after the issue is paginated. If you need an invoice sooner than that, please contact the journal office. **An author with an outstanding debt from a previous paper cannot publish another until the original debt is settled.**

IF YOU ARE PAYING WITH CHECKS OR PURCHASE ORDERS:

- Purchase orders will not be processed without a number.
- Please list vendor as *The University of Chicago Press, 11030 Langley Avenue, Chicago, Illinois 60623*
- If the purchase order is sent separately from this form, it must be marked **"confirming"** and mailed to *Cindy Garrett, Journals Division, The University of Chicago Press, 1427 East 60th Street, Chicago, Illinois 60637*.
- All purchase orders must include the following information:
 - Name of journal, Issue date (month and year—see proofs), Author's name, Amount of the invoice
- Make checks and purchase orders payable to ***The University of Chicago Press***

ELECTRONIC TRANSFER INFORMATION:

- Financial Institution: The Northern Trust Bank, 50 S. LaSalle Street, Chicago IL 60675; Account number: 2725681, Routing number: 071000152, Account name: University of Chicago Press, SWIFT: CNORUS44

Article Information

Volume _____ Issue _____ Month _____ Year _____
Manuscript No. _____

Author(s) _____

Title _____

Open Access: Yes No

Payment Method

1. Institutional Purchase Order No. _____
Purchase Order: attached to come
2. Check or Money Order No. _____
3. Electronic Fund Transfer
4. Credit Card: Visa MasterCard American Express Discover
Name as it appears on card: _____
Card number: _____
Exp. Date: _____ 3-4 Digit Security Code: _____
Signature: _____
Phone number: _____ E-mail: _____

Address of the Person Who Should Receive the Invoice

Mail (REQUIRED): _____

E-mail (REQUIRED): _____